MARTIN MARIETTA ENERGY SYSTEMS LIBRARIES

3 4456 0350998 7

NUREG/CR-5732
(ORNL/TM-11861)

# Iodine Chemical Forms in LWR Severe Accidents

Final Report

Prepared by
E. C. Beahm, C. F. Weber, T. S. Kress, G. W. Parker

**Oak Ridge National Laboratory**

**Prepared for**
**U.S. Nuclear Regulatory Commission**

INFORMATION SERVICES DIVISION
TECHNICAL LIBRARY
Report Collection
Y-12, Building 9711-1, MS-8104
LOAN COPY ONLY

Do NOT transfer this document to any other person. If you want others to see it, attach their names, return the document, and the Library will arrange the loan as requested.

UCN-1624 (3 9-90)

## AVAILABILITY NOTICE

Availability of Reference Materials Cited in NRC Publications

Most documents cited in NRC publications will be available from one of the following sources:

1. The NRC Public Document Room, 2120 L Street, NW., Lower Level, Washington, DC 20555

2. The Superintendent of Documents, U.S. Government Printing Office, P.O. Box 37082, Washington, DC 20013-7082

3. The National Technical Information Service, Springfield, VA 22161

Although the listing that follows represents the majority of documents cited in NRC publications, it is not intended to be exhaustive.

Referenced documents available for inspection and copying for a fee from the NRC Public Document Room include NRC correspondence and internal NRC memoranda; NRC bulletins, circulars, information notices, inspection and investigation notices; licensee event reports; vendor reports and correspondence; Commission papers; and applicant and licensee documents and correspondence.

The following documents in the NUREG series are available for purchase from the GPO Sales Program: formal NRC staff and contractor reports, NRC-sponsored conference proceedings, international agreement reports, grant publications, and NRC booklets and brochures. Also available are regulatory guides, NRC regulations in the *Code of Federal Regulations*, and *Nuclear Regulatory Commission Issuances*.

Documents available from the National Technical Information Service include NUREG-series reports and technical reports prepared by other Federal agencies and reports prepared by the Atomic Energy Commission, forerunner agency to the Nuclear Regulatory Commission.

Documents available from public and special technical libraries include all open literature items, such as books, journal articles, and transactions. *Federal Register* notices, Federal and State legislation, and congressional reports can usually be obtained from these libraries.

Documents such as theses, dissertations, foreign reports and translations, and non-NRC conference proceedings are available for purchase from the organization sponsoring the publication cited.

Single copies of NRC draft reports are available free, to the extent of supply, upon written request to the Office of Administration, Distribution and Mail Services Section, U.S. Nuclear Regulatory Commission, Washington, DC 20555.

Copies of industry codes and standards used in a substantive manner in the NRC regulatory process are maintained at the NRC Library, 7920 Norfolk Avenue, Bethesda, Maryland, for use by the public. Codes and standards are usually copyrighted and may be purchased from the originating organization or, if they are American National Standards, from the American National Standards Institute, 1430 Broadway, New York, NY 10018.


## DISCLAIMER NOTICE

This report was prepared as an account of work sponsored by an agency of the United States Government. Neither the United States Government nor any agency thereof, or any of their employees, makes any warranty, expressed or implied, or assumes any legal liability of responsibility for any third party's use, or the results of such use, of any information, apparatus, product or process disclosed in this report, or represents that its use by such third party would not infringe privately owned rights.

NUREG/CR-5732
ORNL/TM-11861
R3

# Iodine Chemical Forms in LWR Severe Accidents

Final Report

Manuscript Completed: January 1992
Date Published: April 1992

Prepared by
E. C. Beahm, C. F. Weber, T. S. Kress, G. W. Parker

Oak Ridge National Laboratory
Operated by Martin Marietta Energy Systems, Inc.

Oak Ridge National Laboratory
Oak Ridge, TN 37831-6285

**Prepared for**
**Division of Systems Research**
**Office of Nuclear Regulatory Research**
**U.S. Nuclear Regulatory Commission**
**Washington, DC 20555**
**NRC FIN B0854**
**Under Contract No. DE-AC05-84OR21400**

MARTIN MARIETTA ENERGY SYSTEMS LIBRARIES

3 4456 0350998 7

# Abstract

Calculated data from seven severe accident sequences in light water reactor plants were used to assess the chemical forms of iodine in containment. In most of the calculations for the seven sequences, iodine entering containment from the reactor coolant system was almost entirely in the form of CsI with very small contributions of I or HI. The largest fraction of iodine in forms other than CsI was a total of 3.2% as I plus HI. Within the containment, the CsI will deposit onto walls and other surfaces, as well as in water pools, largely in the form of iodide ($I^-$). The radiation-induced conversion of $I^-$ in water pools into $I_2$ is strongly dependent on pH. In systems where the pH was controlled above 7, little additional elemental iodine would be produced in the containment atmosphere. When the pH falls below 7, however, it may be assumed that it is not being controlled and large fractions of iodine as $I_2$ within the containment atmosphere may be produced.

# Contents

Abstract . . . iii

Executive Summary . . . ix

Acknowledgments . . . xi

1 Introduction . . . 1

2 Chemical Forms of Iodine Entering Containment from the Reactor Coolant System . . . 3

2.1 Background . . . 3
2.2 Data Manipulation and Calculational Techniques . . . 3

2.2.1 Adaptation of Data from Source Term Code Package . . . 3

2.3 Iodine-Cesium-Steam-Hydrogen Reactions . . . 9

2.3.1 Sample Calculations . . . 9
2.3.2 Overall Results of Calculations . . . 9

2.4 Reaction of CsOH with Surfaces . . . 10

2.4.1 Deposition of CsOH onto Structural Surfaces . . . 10
2.4.2 Other Reactions of CsOH . . . 10

2.5 Revaporization of CsI from RCS Surfaces . . . 11

2.5.1 Description of Revaporization Process . . . 11
2.5.2 Assessment of Revaporization as a Source of HI . . . 13

2.6 Summary of Iodine Chemical Forms in the RCS . . . 13

3 Iodine Behavior in Containment . . . 15

3.1 Categorization of Iodine Behavior in Terms of Time Intervals During an Accident Sequence . . . 15
3.2 Importance of pH in Determining the Chemical Forms of Iodine in Water Pools . . . 15

3.2.1 Materials That Determine pH in Accident Sequences . . . 15
3.2.2 Nitric Acid Formation and pH Control . . . 16

3.3 Processes That Alter the Chemical Forms of Iodine in Containment . . . 17

3.3.1 Radiolysis . . . 17

3.3.1.1 Description of Calculated Model . . . 17
3.3.1.2 Mass Manipulations . . . 20
3.3.1.3 Gas-Liquid Partitioning . . . 21
3.3.1.4 Gas-Phase Reactions: Formation of Organic Iodides . . . 21
3.3.1.5 Overall Behavior . . . 22

3.3.2 Results of Iodine Behavior in Containment . . . . . 23
3.3.3 Evaporation to Dryness . . . . . 25

4 Technical Findings . . . . . 29

4.1 Perspective and Scope of Study . . . . . 29
4.2 Assessment of Iodine Chemical Forms in the RCS . . . . . 29
4.3 Assessment of Iodine Chemical Forms in Containment . . . . . 29

5 References . . . . . 31

## Appendixes

A Data from Accident Sequence Calculations . . . . . A.1

B Kinetic and Equilibrium Calculations . . . . . B.1

B.1 Kinetics of Cs-I-$H_2$-$H_2O$ Reactions . . . . . B.3
B.2 Equilibrium Calculations in the Cs-I-$H_2$-$H_2O$ System . . . . . B.5

C Fitting of Radiolysis Data . . . . . C.1

D Fission Product Release Tables . . . . . D.1

E Fractional Release Tables . . . . . E.1

## Figures

2.1 Surry TMLB′: temperatures in volumes above core . . . . . 4

2.2 Flow chart of RCS control volumes and variables. Normal type = known data from STCP calculations; italics = quantities to be calculated . . . . . 6

2.3 Surry TMLB′: principal species concentrations in Volume 1 above core . . . . . 7

2.4 Mean residence times in volumes above core for Surry TMLB′ . . . . . 8

3.1 Radiolytic conversion of $I^-$ to $I_2$ [data from C. C. Lin, *J. Inorg. Nucl. Chem.* **42**, 1101 (1980)] . . . . . 18

4.1 Additional atmospheric elemental iodine released . . . . . 30

C.1 Data fitting for radiolytic conversion of $I^-$ to $I_2$ (Data from U.S. Nuclear Regulatory Commission, Regulation Guide 1.4, "Assumptions Used for Evaluating the Potential Radiological Consequences of a Loss-of-Coolant Accident for Pressurized Water Reactors") . . . . . C.4

## Tables


1.1 LWR accident sequences evaluated . . . . . 2
2.1 FACT system output of Grand Gulf TQUV example at 8780 s . . . . . 9
2.2 Simulated core-melt tests conducted in the ORNL 1-kg facility (Boric acid addition to water injected below the bundle) . . . . . 11
2.3 Composition of 10-kg fuel bundle . . . . . 12
2.4 Estimated upper bound on the fraction of iodine as HI due to revaporization of CsI . . . . . 14
3.1 Materials that affect pH in containment water pools . . . . . 16
3.2 Concentrations of $H^+$ and $NO_3^-$ in water due to irradiation . . . . . 17
3.3 Effects of irradiation dose on pH in trisodium phosphate solution . . . . . 17
3.4 Nuclide groupings and group-specific energy deposition rates . . . . . 20
3.5 Data for equilibrium analysis of example sequences . . . . . 24
3.6 Distribution of iodine species for pH controlled above 7 . . . . . 26
3.7 Distribution of iodine species for uncontrolled pH . . . . . 27
3.8 Iodine volatility of $1 \times 10^{-4}$ mol/L CsI solutions during evaporation to dryness . . . . . 28
A.1 Grand Gulf TC—MERGE output data from MARCH2 . . . . . A.3
A.2 Grand Gulf TC—MARCH2 output for input to TRAP-MELT . . . . . A.5
A.3 Grand Gulf TC—MARCH2 output for input to TRAP-MELT . . . . . A.6
A.4 Grand Gulf TQUV—MARCH2 output from MARCH2 . . . . . A.7
A.5 Grand Gulf TQUV—MARCH2 output for input to TRAP-MELT . . . . . A.9
A.6 Grand Gulf TQUV—MARCH2 output for input to TRAP-MELT . . . . . A.10
A.7 Peach Bottom AE—MERGE output for input to MARCH2 . . . . . A.10
A.8 Peach Bottom AE—MARCH2 output for input to TRAP-MELT . . . . . A.11
A.9 Peach Bottom AE—MARCH2 output for input to TRAP-MELT . . . . . A.12
A.10 Peach Bottom TC2—MERGE output from MARCH2 . . . . . A.13
A.11 Peach Bottom TC—MARCH2 output for input to TRAP-MELT . . . . . A.15
A.12 Peach Bottom TC—MARCH2 output for input to TRAP-MELT . . . . . A.16
A.13 Sequoyah TB—MERGE output from MARCH2 . . . . . A.17
A.14 Sequoyah TB—MARCH2 output for input to TRAP-MELT . . . . . A.18
A.15 Sequoyah TB—MARCH2 output for input to TRAP-MELT . . . . . A.19
A.16 Surry TMLB′—MERGE output from MARCH2 . . . . . A.20
A.17 Surry TMLB′—MARCH2 output for input to TRAP-MELT . . . . . A.21
A.18 Surry TMLB′—MARCH2 output for input to TRAP-MELT . . . . . A.21
A.19 Surry AB—MARCH2 output for input to TRAP-MELT . . . . . A.22
A.20 Surry AB—MARCH2 output for input to TRAP-MELT . . . . . A.22
A.21 Surry AB—MARCH2 output for input to TRAP-MELT . . . . . A.23
A.22 Grand Gulf—Compartment volumes for sequences TC and TQUV . . . . . A.23
A.23 Peach Bottom—Compartment volumes for sequences TC and AE . . . . . A.24
A.24 Sequoyah—Compartment volumes for sequence TBA . . . . . A.24
A.25 Surry—Compartment volumes for sequences AB and TMLB . . . . . A.24
B.1 Reaction rate constants . . . . . B.4
B.2 Standard free energy of reaction 500 to 1200 K (441 to 1701°F) written as $\Delta G^{\circ}_{F_{rxn}} = a + bT$, exothermic reaction expressed left to right (Energy in joules) . . . . . B.5
C.1 Radiolysis data for formation of $I_2$ . . . . . C.3
D.1 Fission product inventories for selected plants . . . . . D.3
D.2 Bounding values for fractions of core inventory released into containment . . . . . D.4
E.1 Grand Gulf — fractional releases and energy deposition rates . . . . . E.3
E.2 Peach Bottom — fractional releases and energy deposition rates . . . . . E.4
E.3 Sequoyah — fractional releases and energy deposition rates . . . . . E.5
E.4 Surry TMLB′ — fractional releases and energy deposition rates . . . . . E.6

# Executive Summary

The analyses in this study were based on quantitative (calculated) results of seven severe accident sequences for light water reactor (LWR) nuclear power plants. These sequences represent a wide range of conditions that are significant risks. Both high- and low-pressure sequences were chosen for three principal plant types; a single sequence was considered for the PWR ice condenser. Each sequence was evaluated by the Source Term Code Package (STCP), and the thermal hydraulics has been documented in previous NRC reports.[1,2] The issue that has been addressed is the chemical forms of iodine in the reactor coolant system (RCS) and in containment — not the ultimate disposition of these chemical forms.

In an LWR accident sequence, fission products released from the core will undergo changes in temperature and concentration as they pass through regions of the RCS. A chemical kinetic model used 20 reactions to determine the control volume where an equilibrium of the iodine, cesium, hydrogen, and steam species becomes "frozen." This means that the temperatures and concentrations of species in subsequent control volumes are not sufficient to reach an equilibrium in the mean residence time available. The "frozen" equilibrium is the species distribution entering containment. Separate equilibrium calculations were performed, using the FACT system,[3] to obtain the distribution of iodine species. The FACT system was chosen in this study because it can be used by anyone who wishes to examine the calculations and its data base contains only assessed data.

In six of the seven calculations, iodine entering the containment from the RCS was almost entirely in the form of CsI; the contributions of I or HI were <0.1% of the overall percentage of iodine.

During the second half of the Surry AB sequence, there is a period during which temperatures in the core region are predicted to be in excess of 2000 K (3141°F) and subsequent volumes of the upper grid plates and guide tubes are at temperatures of only ~500 K (441°F). Under such conditions, the equilibrium compositions in the core region would be "frozen" by the rapid decrease in temperature. For this sequence, the overall iodine distribution was 2.8% as I, 0.4% as HI, with the remainder as CsI. Thus, a total of 3.2% as I plus HI was the largest fraction of iodine in a form other than CsI calculated to enter containment from the RCS in this study.

Once within the containment, CsI is expected to deposit onto interior surfaces and dissolve in water pools, forming iodide ($I^-$) in solution. The dissolution of HI and $HNO_3$ (produced by irradiation of $N_2$ in the atmosphere) and the hydrolysis of $I_2$ tend to acidify films and pools of water.

Iodine behavior in containment was evaluated during the early stage of an accident sequence, up to ~1200 min. If pH is controlled in containment water pools so that it stays above 7, a reasonable value for the fraction of $I^-$ converted to $I_2$ is $3 \times 10^{-4}$. This yields a small production of volatiles for PWRs, but virtually none for BWRs. Thus, if pH is maintained at 7 or above, only a small additional amount of $I_2$ is indicated to enter the gas phase in PWR systems.

If the pH drops below 7 (assumed uncontrolled pH), a larger fraction of aqueous $I^-$ will be converted to $I_2$. Evaporation of this volatile species so as to maintain equilibrium partitioning will result in greater atmospheric $I_2$, which, in turn, will yield higher organic iodide concentrations. As expected, the levels of airborne iodine volatiles are much higher than in the pH-controlled case, indicating almost complete conversion for PWRs.

The gaseous $I_2$ fraction is considerably higher in PWRs than in BWRs because of the large water volumes in the latter, which both lower the dose rate and retain greater quantities of dissolved $I_2$.

In addition, organic iodide is present in PWRs at about 0.5% of core inventory; in BWRs, this value is closer to 0.1%. The $I_2$ generated by the radiolytic conversion of $I^-$ in containment pools dominates the amount released directly from the RCS as $I_2$. In addition, due to the equilibrium assumption, the presence of some $I_2$ already airborne will result in less evaporation of $I_2$ formed radiolytically. Hence, for the case of uncontrolled pH, the cumulative total

is well represented by the equilibrium amount formed within containment.

The production of $I_2$ in containment will be directly related to the pH levels of the water pools. There is a significant difference in the amount of $I_2$ between the uncontrolled-pH and the controlled-pH cases. A major uncertainty in fixing the production of volatile iodine chemical forms in containment involves the extent of evaporation to dryness. At a minimum, 2 to 20% of the iodine in water pools that have evaporated would have been converted to a volatile form, most likely as $I_2$.

# Acknowledgments

The authors acknowledge the aid of Michael Brown, of Thurso, Scotland, who wrote the routine used with the FACSIMILE code and performed scoping calculations for this study. We also wish to express gratitude to Betty Drake for preparing the manuscript. In addition, we appreciate the assistance of Vladimir Kogan of Battelle Columbus Laboratories in obtaining data on accident sequences.

# 1 Introduction

In the past 10 years, studies of iodine behavior in containment under accident conditions have identified a variety of chemical and physical interactions that will determine the forms of iodine and environments where reactions may occur.[4-7] In general terms, the ability to predict iodine behavior is now more limited by knowledge of the environment in which the iodine is present than by deficiencies in understanding what iodine will do in a given set of environments. Thus, with only a few exceptions, the prediction of chemical form or magnitude of iodine released from containment is limited by the lack of information on the materials and environments involved in iodine reactions in the containment, as well as by uncertainty in the chemical forms and amounts of iodine that enter the containment. For example, it has been found that boric acid and borates are important in determining the chemical forms of iodine in the RCS and in the containment. However, the location, amounts, and type of borate are not well defined in severe accident sequences. A number of tests were performed to examine organic iodide formation with a variety of materials. However, it is not known what organic material will be present and in what form it will exist for a given reactor plant and accident sequence.

Some information on iodine reactions has not yet been put into models and implemented in computer codes. The disparity between information on reactions and models for a computer code is best illustrated by the effect of water radiolysis on iodine chemical forms. Experimental data show that radiolysis can control the chemical forms of iodine in water. Models were developed to calculate water radiation dose rates and pH in severe accident sequences. Modeling of iodine radiolysis at a pH and dose rate in terms of individual reaction rate constants has proven to be extremely difficult because it requires expressions for (1) radiolysis of water, (2) iodine hydrolysis, and (3) the interaction of iodine species with water radiolysis products.

In summary, uncertainties in iodine chemical forms in containment stem principally from uncertainties in the (1) chemical forms and amounts of iodine that enter containment, (2) conditions and materials in which iodine interacts, and (3) lag between obtaining data and implementing it in computer models and codes.

Regulatory Guides 1.3[8] and 1.4[9] state the following:

(1) Fifty percent of the maximum iodine inventory of the reactor core is released to the primary reactor containment; 25% is available for leakage.

(2) Of this 25%, 91% is in the form of elemental iodine, 5% is in the form of particulate iodine, and 4% is in the form of organic iodide.

Iodine is assumed to enter containment in the forms and amounts stated above with neither physical nor chemical changes occurring in containment. However, present knowledge may not support this distribution of iodine forms and the static state throughout the duration of an accident.

It is anticipated that a more "realistic" representation of the chemical speciation of fission product iodine would likely have the following characteristics:

(1) an initial release of some combination of particulate iodine (CsI) and gaseous iodine (HI) or (I), with the largest proportion being particulates

(2) a continuous re-release of molecular iodine that would arise from "revolatilization" from water repositories and would include some small complement of organic iodine

Table 1.1 lists the seven calculated LWR severe accident sequences considered in this analysis; these sequences involve a wide range of conditions that represent significant risks. Both high- and low-pressure sequences were chosen for three principal plant types; a single sequence was considered for the PWR ice condenser. Each sequence was evaluated by the STCP and has been documented in previous NRC reports.[1,2]

Table 1.1 LWR accident sequences evaluated

| Plant | Reactor type | Accident | Accident type | Documentation* |
|---|---|---|---|---|
| Grand Gulf | BWR — Mark III | TC<br>(ATWS) | High pressure | BMI-2104, Vol. III |
| | | TQUV<br>(No makeup water) | Low pressure | BMI-2104, Vol. III |
| Peach Bottom | BWR — Mark I | TC2<br>(ATWS) | High pressure | NUREG-4624, Vol. I |
| | | AE<br>(LOCA, no ECCS) | Low pressure | BMI-2104, Vol. II |
| Sequoyah | PWR — ice condenser | TBA | Low pressure | NUREG-4624, Vol. II |
| Surry | PWR — large containment | TMLB′<br>(Station blackout) | High pressure | BMI-2104, Vol V |
| | | AB<br>(LOCA, no ECCS)<br>(Station blackout) | Low pressure | BMI-2104, Vol. V |

*See References 1 and 2 for complete reference description.

# 2 Chemical Forms of Iodine Entering Containment from the Reactor Coolant System

## 2.1 Background

The chemical forms of iodine in the RCS are closely tied to the chemical forms of cesium. The relationship between cesium and iodine in the RCS can be illustrated by the following reaction

$$CsI + H_2O \rightleftharpoons CsOH + HI \qquad (1)$$

The reaction of cesium iodide (CsI) with steam ($H_2O$), as shown in Equation 1, is the reverse of an acid-base reaction and, thus, is unlikely to proceed unless one or both products are removed. Reactions of CsOH, which tend to lower the partial pressure of CsOH, shift the equilibrium to the right and enhance the formation of HI.

At temperatures in excess of 1800 K (2781°F) and at low hydrogen pressures, iodine as I, rather than HI, is the favored product of the reaction between CsI and $H_2O$

$$CsI + H_2O \rightleftharpoons CsOH + I + \frac{1}{2}H_2 \qquad (2)$$

Thus, iodine chemical forms other than CsI are favored when steam pressures are much greater than cesium hydroxide pressures.

Fission products released from the core will undergo changes in temperature and concentration as they pass through regions of the RCS. A chemical kinetic model used 20 reactions to determine the control volume where an equilibrium of the iodine, cesium, hydrogen, and steam species becomes "frozen." This means that the temperatures and concentrations of species in subsequent control volumes are not sufficient to reach an equilibrium in the mean residence time available. Separate equilibrium calculations were run, using the FACT system,[3] to obtain the distribution of iodine species. The FACT system was chosen for this study because it can be used by anyone who wishes to examine the calculations and its data base contains only assessed information.

## 2.2 Data Manipulation and Calculational Techniques

### 2.2.1 Adaptation of Data from Source Term Code Package

In order to evaluate the chemistry in the RCS, it is necessary to specify the thermal-hydraulic conditions under which reactions would occur. This has been undertaken for each of the accident sequences in Table 1.1 using data from the STCP calculations. Where possible, detailed transient data were taken from the original computer output; otherwise, values were derived from tables or estimated from graphs in the sequence documentation.[1,2] A listing of all the data used is contained in Appendix A.

The chemical equilibrium is calculated in each relevant RCS control volume for the individual sequences. This requires a description of the thermodynamic conditions that occur during various phases of accident progression and a measure of the time span over which such conditions hold.

The MARCH2[10] code generates a special output file that provides input for the TRAP-MELT[11] code. This file was used to identify time-varying values of temperature and pressure in the RCS. Each control volume in the RCS remains constant, and the values used are given in Appendix A. Figure 2.1 illustrates the temperature history of the first two control volumes above core in the Surry TMLB′ accident sequence, where time 0 is at the start of core melting. The figure shows phases of constant or slowly changing behavior in addition to periods of large swings in magnitude. Other sequences exhibit similar patterns.

In addition to $T$, $P$, and $V$, chemical equilibria are dependent on the molar inventories $n_i$ of constituent species $H_2$, $H_2O$, I, and Cs. These inventories also vary during the transient and must be obtained for each control volume. Such quantities are calculated

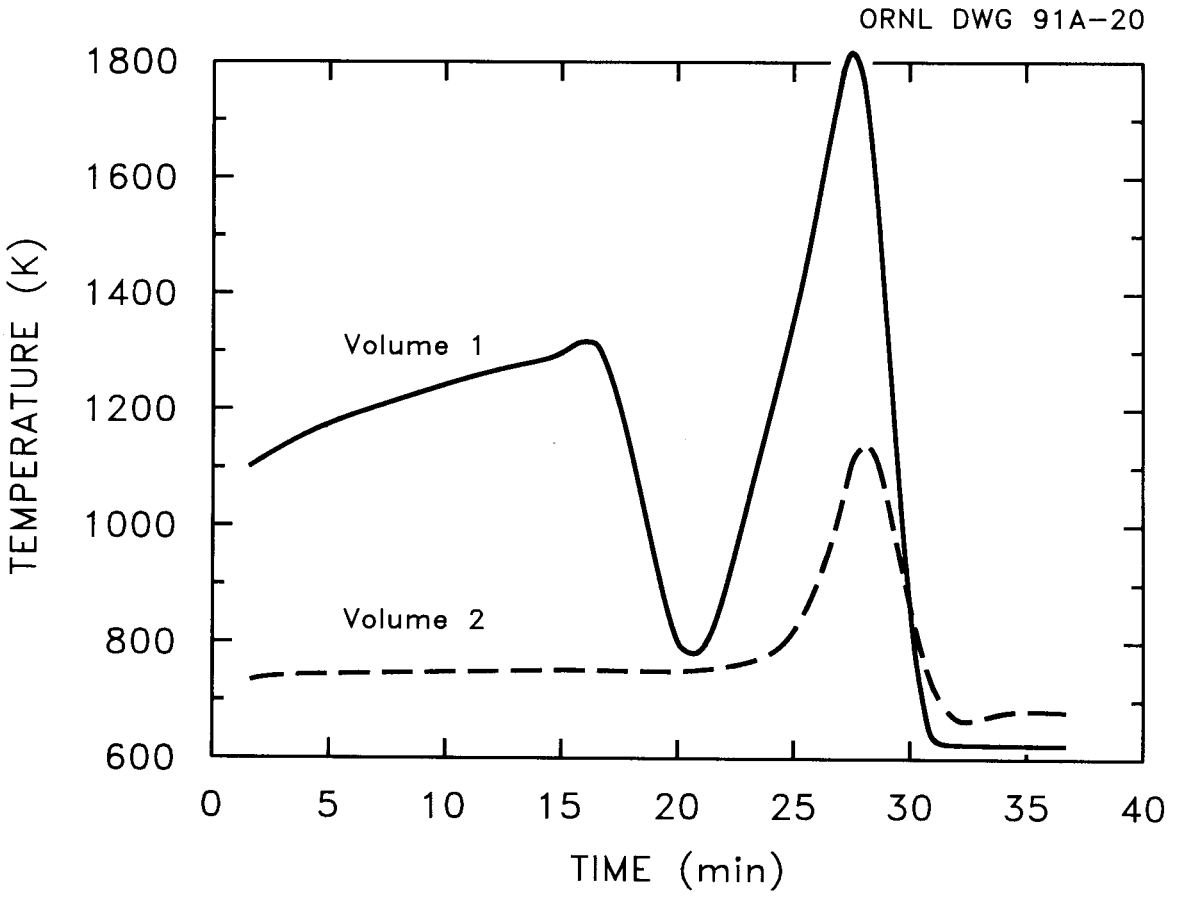


**Figure 2.1 Surry TMLB′: temperatures in volumes above core**

since they are not directly available from STCP results. Mass flows of $H_2$ and $H_2O$ and release rates of CsI and CsOH from the core are converted into molar flows ($g_{i0}$, $i$ = 1, 2, 3, 4) of $H_2$, $H_2O$, I, and Cs. These are assumed to directly enter the first control volume above the core. A simple schematic of the system of above-core control volumes is shown in Figure 2.2. Known data are given in normal type, and quantities to be calculated are shown in italics. Although only two control volumes are shown, additional ones could be added (and were for most of the sequences in this study); treatment would be analogous to the second volume in the figure.

Within each control volume, temperature and pressure are assumed to be uniform spatially and constant over computational time intervals (time intervals must be specified small enough to make this valid). From the ideal gas law, the total molar inventory must then also be constant since $n = PV/RT$. This implies that the molar flow (g-mol/s) into a control volume must equal the molar flow out

$$\sum g_{i1} = \sum g_{i2} = \sum g_{i0} = g \qquad (3)$$

Since the inlet flows $g_{i0}$ are known (cf. Figure 2.2), the total flow $g$ can be easily obtained. The volumetric flow $v_j$ from control volume $j$ ($m^3/s$) is, then

$$v_j = g\,\frac{RT_j}{P} \qquad (4)$$

and the volume fractional flow from volume $j$ ($s^{-1}$) is

$$f_j = \frac{v_j}{V_j} = g\,\frac{RT_j}{PV_j} \qquad (5)$$

Assuming well-mixed control volumes, the flow (mol/s) of constituent $i$ from volume $j$ is represented by

$$g_{ij} = f_i\, n_{ij} \qquad (6)$$

where the molar inventories $n_{ij}$ are updated at each time step by a simple balance equation

$$n_{ij}^{new} = n_{ij}^{old} + \Delta t\,(g_{ij-1} - g_{ij}) \qquad (7)$$

Using this procedure, molar inventories were calculated in each control volume downstream from the core, as were the molar concentrations $C_{ij} = n_{ij}/V_j$. As an example, Figure 2.3 shows the time variation of principal species concentrations for the first control volume above core in the Surry TMLB′ sequence. These concentrations, together with temperature and pressure values, were subsequently used to estimate the equilibrium distributions of chemical species, as described in Section 2.3.1. It is important to note that the equilibrium chemistry was completely decoupled from the mass transfer processes (i.e., no chemical reactions were considered in the flow calculations).

The mean residence time (s) for flow through a control volume is simply the inverse of the fractional flow

$$\tau_j = \frac{1}{f_j} \qquad (8)$$

Figure 2.4 shows this quantity for each of the two control volumes above core in the Surry TMLB′ sequence. As described in Section 2.3.1, a mean residence time >1 s is usually sufficient to attain equilibrium for regions with a sufficiently high temperature. The mean residence time is greater than 1 s for both volumes, although control volume 1 approaches this limit briefly at about 30 min.

The simplicity of this method introduces some uncertainty into the results. However, this uncertainty is generally far less than that due to the input data itself. The time steps were chosen small enough to reduce calculational error to relative insignificance when compared with other sources of error; hence, the chemical reactions may have a slight effect on pressure and temperature, but this is not expected to be significant in altering the inventory and flow patterns. Thus, the results provide a reasonable picture of the chemical thermodynamic conditions in each control volume as the transients progress.

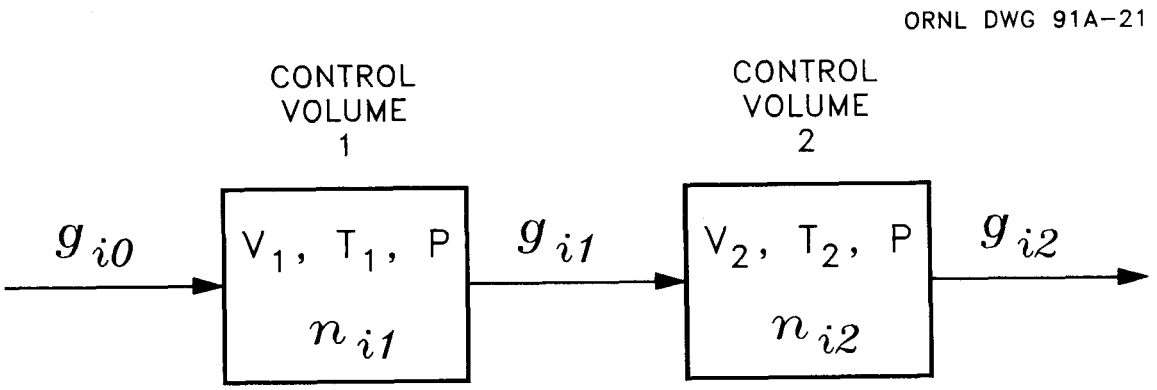


Figure 2.2 Flow chart of RCS control volumes and variables. Normal type = known data from STCP calculations; italics = quantities to be calculated

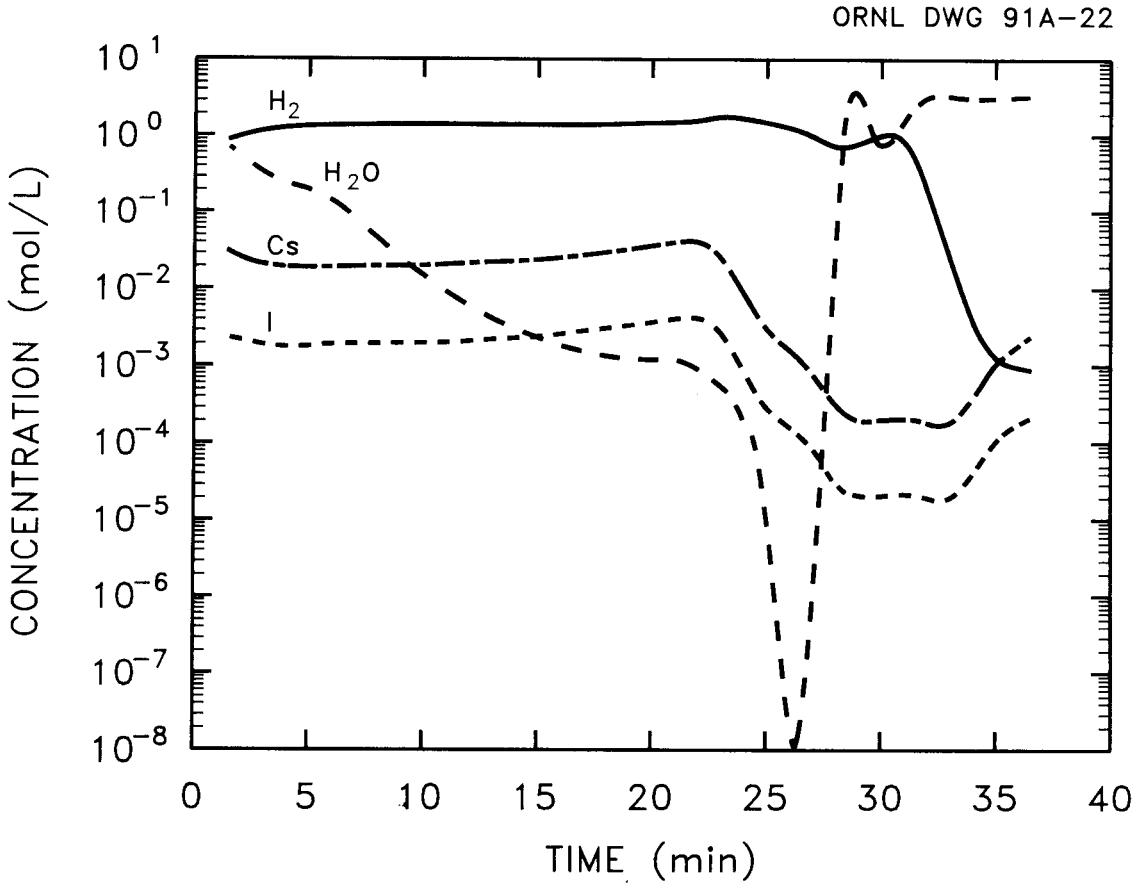


**Figure 2.3 Surry TMLB′: principal species concentrations in Volume 1 above core**

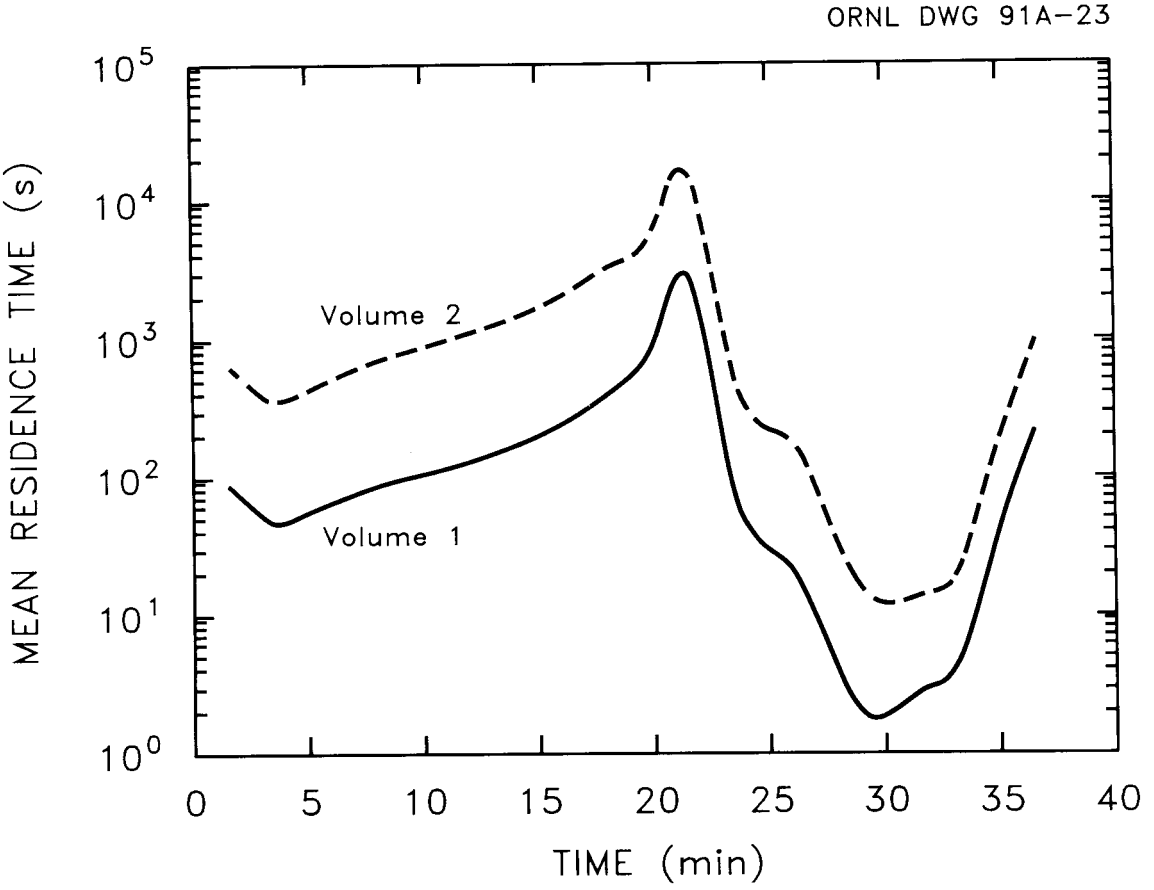


**Figure 2.4 Mean residence times in volumes above core for Surry TMLB′**

## 2.3 Iodine-Cesium-Steam-Hydrogen Reactions

### 2.3.1 Sample Calculations

Kinetic and equilibrium calculations were carried out at frequent intervals during the seven accident sequences. The use of these procedures can be illustrated with the Grand Gulf TQUV sequence at 8780 s. Temperatures of the control volumes are shown in Table 2.1. Kinetic calculations, using the FACSIMILE[12] code, indicated that the equilibrium was not attained in the upper annulus at 907 K (1173°F). However, equilibrium was rapidly attained in the higher-temperature regions. The results of the equilibrium calculations are given in Table 2.1. In the core region, some I and HI were indicated along with CsI. The predominance of I over HI here is the result of reaction 2 being dominant over reaction 1 at the relatively high temperature of this region. Very little I or HI was indicated in the steam separator volume, and essentially only CsI was present in the steam dryers. In this example, the equilibrium was "frozen" at 1180 K (1665°F) in the steam dryer volume because this is the lowest temperature where equilibrium could be attained. If the equilibrium had "frozen" in the core region by quenching from its high temperature without changing composition, then the distribution of iodine species would have been different (see Table 2.1). Calculational techniques used in the seven accident sequences are discussed in Appendix B.

**Table 2.1 FACT system output of Grand Gulf TQUV example at 8780 s**

| Control volumes | Percent CsI | Percent I | Percent HI | Temperature (K) | Temperature (°F) |
|---|---|---|---|---|---|
| Core region | 91.0 | 7.5 | 1.5 | 2047 | 3225 |
| Steam separators | 99.96 | 0.01 | 0.03 | 1398 | 2057 |
| Steam dryers | ~100.0 | <0.01 | <0.01 | 1180 | 1665 |
| Upper annulus | Not at equilibrium | | | 907 | 1173 |

### 2.3.2 Overall Results of Calculations

In six of seven calculations, the iodine was almost entirely in the form of CsI; the contribution of I or HI was <0.1% of the overall percentage of iodine.

During the second half of the Surry AB sequence, there is a period during which temperatures in the core region are in excess of 2000 K (3141°F) and subsequent volumes of the upper grid plates and guide tubes are at temperatures of only ~500 K (441°F). Because of this, equilibrium compositions in the core region would be "frozen" in by the rapid decrease in temperature. For this sequence, the overall iodine distribution was 2.8% as I and 0.4% as HI, with the remainder as CsI. Thus, a total of 3.2% as I plus HI was the largest fraction of iodine in a form other than CsI in this study.

These calculations considered only reactions involving cesium, iodine, hydrogen, and species, as shown in Appendix B, but covered a wide range of temperatures, hydrogen concentrations, steam concentrations, and fission product concentrations. However, deposition on surfaces and reactions with surfaces were not included in these calculations. Very few specific experimental data about surface

interactions of fission products are available. The effect of these interactions on iodine chemical forms must be carried out with scoping or bounding calculations rather than detailed sequence specific evaluations that were performed for the reactions of iodine and cesium species with steam and hydrogen.

## 2.4 Reaction of CsOH with Surfaces

### 2.4.1 Deposition of CsOH onto Structural Surfaces

Of the possible reactions of CsOH in the RCS, the reaction with structural surfaces is the most amenable to evaluation. Johnson et al.[13] have studied the deposition of CsOH on oxidized stainless steel surfaces. They used the following simple expression to relate the thermodynamic activity of CsOH to the surface concentration

$$a = 0.5 \exp\left\{\left(98.5 - \frac{3.84 \times 10^4}{T}\right)(x - 0.28)\right\} \qquad (9)$$
$$x < 0.28$$

where $a$ and $x$ are the surface activity (atm) and concentration (mg/cm$^2$), respectively. The reaction of interest with stainless steel may be written as

$$\text{CsOH (surface)} \rightleftharpoons \text{CsOH (gas)} \qquad (10)$$

Thermochemical data obtained from the FACT system[3] give the respective equilibrium constants for the reactions in Equations 1 and 9 as

$$K_1 = \frac{P_{CsOH}}{P_{H_2O}} \frac{P_{HI}}{P_{CsI}} = \exp\left(-1.407 - \frac{1.626 \times 10^4}{T}\right) \qquad (11)$$

$$K_9 = \frac{P_{CsOH}}{a} = \exp\left\{1.189 \times 10^1 - \frac{1.500 \times 10^4}{T}\right\} \qquad (12)$$
$$900 \le T \le 1263$$

Calculations using Equations 9, 11, and 12, together with mass balances on cesium and iodine, indicate that the amount of HI formed due to the CsOH surface reaction is less than 0.6% for each of the accident sequences studied. This is because $P_{CsOH}$ must be very small if the ratio $P_{HI}/P_{CsI}$ is large enough to be significant. However, if $P_{CsOH}$ is very small, then so is $x$; hence, very little surface reaction could occur.

### 2.4.2 Other Reactions of CsOH

Other reactions of CsOH may also remove it from the vapor phase, but there is generally a lack of information on the amounts and locations of other reactants. For example, several cesium borates may form in the reaction of CsOH with boric acid or boron oxide. The formation of cesium metaborate ($CsBO_2$) may occur by the following reaction

$$CsOH + HBO_2 \rightleftharpoons CsBO_2 + H_2O \qquad (13)$$

At equilibrium at 1000 K (1341°F), the pressure of CsOH may be written as

$$P_{CsOH} = \sim 1.6 \times 10^{-11} \cdot \frac{P_{H_2O}}{P_{HBO_2}} \qquad (14)$$

If sufficient meta-boric acid ($HBO_2$) were available, it could result in a lowering of the vapor pressure of CsOH.

Two simulated core-melt tests were run at ORNL to assess boric acid volatility and the potential for vapor interactions with CsI. Two different sized simulant fuel bundles were used—nominally 1 and 10 kg. The smaller, 1-kg, fuel simulant bundle consisted of 12 zirconium tubes (10.16 cm long) with 0.247 kg end caps, 0.093 kg stainless steel grids, 0.0185 kg Inconel grids, and 0.585 kg $UO_2$ pellets. There were no added Cs or I species in the small bundle test. The test was performed by inductively heating the fuel bundle while injecting feedwater containing 2000 ppm boric acid into the bottom of the bundle. In this test, it was found (see Table 2.2) that during the lower-temperature heating steps up to 1600°C, ~10% of the boron was transported through the bundle and was captured downstream as boron oxide. As the temperature was increased to partial melting of the bundle, the collected $B_2O_3$ decreased. This decrease was

**Table 2.2 Simulated core-melt tests conducted in the ORNL 1-kg facility (Boric acid addition to water injected below the bundle)**

| | | Boron collected as $B_2O_3$ | |
|---|---|---|---|
| Heating step | Total boron present* (g) | Filter (%) | Wash (%) |
| A (1600°C) | 0.034 | 10.37 | 0.0 |
| B (1800°C) | 0.088 | 5.5 | 0.68 |
| C (2400°C) | 0.142 | 0.024 | 0.009 |

*As boric acid in water used for steam generation.

attributed to increased reactivity of the boron oxide with the hot fuel and clad oxides.

The composition of the 10-kg fuel bundle is shown in Table 2.3. Note that in this test, CsI was added to 12 of the 60 simulant fuel rods in a limited region near the bundle centerline. Excess cesium was not added.

The 10-kg test was conducted at a bundle centerline temperature limit of 1600°C, which was reached in ~30 min and maintained for an additional 30 min. During this time, 365 mL of boric acid solution containing 3.83 g of $H_3BO_3$ was added to the steam generator porous media below the fuel bundle. Hydrogen release measured 326 L, which would be equivalent to 72% conversion of the water and ~30% reaction of the Zircaloy in the bundle.

Analytical results from X-ray diffraction showed that white solids observed plated out on the quartz chimney were nearly pure CsI with no detectable $B_2O_3$. Chemical analysis of the washings from the system indicated that nearly half of the CsI had vaporized and that no boron-containing materials were present. This complete failure to find any $B_2O_3$ downstream of the bundle was somewhat unexpected since the 1-kg test had resulted in some penetration of boron oxide. It is likely that the extra length of the 10-kg system prevented penetration by the reaction of $B_2O_3$ with $ZrO_2$. A sample analysis of a white oxide (a thin ring of mixed $ZrO_2$ and $B_2O_3$) in a very highly refractory solid solution on the oxidized clad surface was estimated to account for about one-third of the total boron added. The remainder of the boron oxide appeared to be associated with the porous $ZrO_2$ steam generator base at the bottom of the bundle. A test scrubber that had been operated continuously on a diverted part of the hydrogen/steam flow showed no evidence of volatile (nonparticulate) iodine.

Similar results were subsequently obtained in a test with silver vaporized in a 10-kg bundle containing Ag-In-Cd alloy control rod simulants. In the latter case, cadmium vapor was observed downstream, but the silver did not penetrate out of the bundle—presumably because of interactions with Zircaloy.

Based on these results, it is highly likely that boric acid covaporized from residual water below the core in severe accidents will be tied up by the Zircaloy in the lower regions of the core and will not be available airborne to affect the chemical form of the released iodine.

## 2.5 Revaporization of CsI from RCS Surfaces

### 2.5.1 Description of Revaporization Process

During an accident sequence, CsI may condense on RCS surfaces. If the temperature increases later in the sequence, the CsI may revaporize into a gas with very little cesium hydroxide. The revaporization of CsI can be expressed as

**Table 2.3 Composition of 10-kg fuel bundle**

| Item | Weight* (g) |
|---|---|
| 60** — Zircaloy tubes | 2181.0 |
| 120 — Zircaloy end caps | 503.6 |
| 3 — Stainless steel grids | 342.0 |
| 1 — Inconel grid | 112.0 |
| 4 — Stainless steel supports and screws | 58.5 |
| 2 — Stainless steel lifts and screws | 9.0 |
| $UO_2$ pellets | (N.W.) 7464.0<br>(E.W.) 6739.9 |
| $UO_2$ powder | (N.W.) 1201.9<br>(E.W.) 1059.5 |
| $SrCO_3$ | 3.00 |
| $BaCO_3$ | 4.05 |
| $La_2O_3$ | 2.28 |
| $Eu_2O_3$ | 0.21 |
| $Sm_2O_3$ | 1.12 |
| $CeO_2$ | 4.87 |
| Mo | 4.70 |
| Te | 0.82 |
| Ru | 5.16 |
| CsI† | 0.85 |

*N.W. = net weight; E.W. = uranium element weight.
**Twelve of these tubes had three horizontal slits each, 0.010 in. wide × 1 in. long, and 120° apart in their midsection.
†CsI mixed with 300 g $UO_2$, rare earths, and metal powders was added to the ~1-in. section of the 12 tubes.

$$\text{CsI (liquid)} \rightleftharpoons \text{CsI (gas)} \qquad (15)$$

The vapor pressure of CsI, calculated with data obtained from the FACT system,[3] is

$$P_{CsI} = \exp\left[\frac{-2.021 \times 10^4}{T} + 1.307 \times 10^1\right] \qquad (16)$$
$$T = 1000 - 1553 \text{ K}$$

In Equation 1, a mole of CsOH would be produced for every mole of HI. Assuming that this is the only CsOH (gas) in the system for the sake of a bounding calculation, the equilibrium constant for reaction 1 may be arranged as

$$P_{HI}^2 = P_{CsI} \cdot P_{H_2O} \exp\left\{-\left(\frac{1.622 \times 10^4}{T} + 1.467\right)\right\} \qquad (17)$$
$$T = 1000 - 1553 \text{ K}$$

### 2.5.2 Assessment of Revaporization as a Source of HI

From Equation 17, $P_{HI}$ may be calculated if $P_{H_2O}$ is known or assumed and $P_{CsI}$ is calculated from Equation 16. The calculated percentages of iodine as HI when $P_{H_2O}$ = 1 atm varied from 0.5% at 1000 K to 0.25% at 1553 K. At higher steam pressures, proportionately higher percentages as HI may occur.

To assess an upper bound on the extent of HI formation by revaporization of CsI, the following assumptions are made:

(1) The temperature of revaporization is the temperature where equilibrium was "frozen."

(2) The steam pressures are those obtained from the seven accident sequences.

(3) The only CsOH (gas) in the system is that produced by Equation 1 and is, mole for mole, the same as HI. All other cesium was somehow removed (i.e., vented).

(4) All of the iodine deposited on the surface and was subject to revaporization as described by Equations 15 and 16.

Table 2.4 indicates the estimated upper bounds on the fraction of iodine as HI that results from these assumptions. The highest percentages as HI were obtained from those accidents in which steam pressures were >1 atm for a significant time during the sequence. These upper bounds probably overestimate the formation of HI in several ways:

(1) It is not likely that all iodine would deposit as CsI and be subject to later revaporization.

(2) The steam pressures used in the calculations were those of the accident sequences. Revaporization could occur after steam pressures had decreased.

(3) The cesium hydroxide pressure would most likely be greater than the HI pressure. As described in Section 2.4.1, it would be difficult to reduce CsOH pressures low enough to influence HI formation by deposition of cesium on stainless steel.

## 2.6 Summary of Iodine Chemical Forms in the RCS

Iodine entering containment from the RCS should be predominantly in the form of CsI. The examination of Cs-I-$H_2O$-$H_2$ interactions for seven accident sequences gave a maximum of 3.2% iodine as I plus HI, with the remainder as CsI. There are some uncertainties in the reactions of CsOH with oxides, as well as in the revaporization of CsI, that produce uncertainties in the extent to which iodine may exist in a form other than CsI. Cesium needs to be removed from reactions involving iodine if very much iodine is to be in a form other than CsI.

Based on this analysis, the chemical forms of iodine entering containment from the RCS may reasonably be described as a maximum of 5% as elemental iodine and HI, with not less than 1% as either elemental iodine or HI. The remaining 95% would be CsI.

**Table 2.4. Estimated upper bound on the fraction of iodine as HI due to revaporization of CsI**

| Accident sequence | Estimated percentage of iodine as HI* |
|---|---|
| Grand Gulf TC | 0.3 |
| Grand Gulf TQUV | 0.4 |
| Peach Bottom AE | 0.6 |
| Peach Bottom TC2 | 3.1 |
| Sequoyah TB | 2.4 |
| Surry TMLB' | 3.8 |
| Surry AB | 0.03 |

*Note: See Section 2.5.2 for a list of assumptions used in calculating these estimated values.

# 3 Iodine Behavior in Containment

## 3.1 Categorization of Iodine Behavior in Terms of Time Intervals During an Accident Sequence

Based on TRENDS models, calculations of iodine behavior for NUREG-0956,[14] and information from large-vessel tests[15-18] as well as from the accident at TMI-2, the iodine behavior may be separated, by time, into three categories: (1) from initial release into containment up to 1000 to 1200 min following initiation of the accident, (2) from 1000 to 1200 min to ~2 to 3 weeks, and (3) for times greater than ~3 weeks.

Category 1. Iodine Behavior. In this time interval, the uncertainty in the amount and chemical forms that enter containment is most important. The upper time limit for this category is the time when airborne aerosol concentrations have been substantially reduced from their peak values. The source term calculations in previous reports[1,2] stopped in the range of 1000 to 1200 min.

All of the chemical and physical interactions of HI are expected to occur during this time interval. Events leading to the formation of $I_2$ by radiolysis would also occur in this interval and the next time interval as well. Thus, during this period, all material of importance to iodine reactions is expected to deposit in water pools or onto surfaces, all gaseous iodine-aerosol interactions are expected to take place, and all HI effects, except for those related to pH, are expected to occur.

Category 2. Iodine Behavior. In this time interval, vapor-phase iodine will consist of $I_2$ produced by radiolysis and partitioned between aqueous solution and the gas, as well as organic iodide. Iodine will also be found in aqueous solution in forms that are determined both by radiolysis and by pH and deposited on structural surfaces. In this time interval, the chemical forms of iodine should not be closely related to the chemical forms that entered containment from the RCS because the iodine would have interacted with a surface and/or dissolved in water.

Category 3. Iodine Behavior. At long times after a severe accident, gas-phase iodine is expected to be dominated by organic iodide with a small contribution from $I_2$. Approximately 15 months following the accident at TMI-2, the concentration of $^{129}I$ in containment gas was $3.3 \times 10^{-12} \pm 8.9 \times 10^{-13}$ mol I/L.[19] Methyl iodide is an "ubiquitous" halocarbon that is present in the atmosphere at concentrations which vary somewhat with distance from the ocean. In a study of eight locations in the United States, the overall mean concentration was $\sim 2 \times 10^{-12}$ mol $CH_3I$/L.[20] Thus, the long-term organic iodide concentration in containment will probably be on the order of $10^{-12}$ mol I/L. Iodine behavior and distribution, in the long term, are expected to have little relationship to the chemical forms or amounts released into containment because the iodine would have had time to deposit on surfaces or in water pools and the environmental conditions in containment would prevail in determining the chemical forms.

## 3.2 Importance of pH in Determining the Chemical Forms of Iodine in Water Pools

### 3.2.1 Materials That Determine pH in Accident Sequences

Results of various experiments have shown that solution pH is the major factor in determining the amount of $I_2$ and organic iodide formation in solution.[4] Materials that can determine pH in containment water pools are given in Table 3.1. This list includes both acidic and basic materials. In situations in which no chemical additives are present to control pH, the amounts of HI, cesium borate or hydroxide, and boron oxides reaching a sump will initially determine pH. In some sequences, the core-concrete interaction would produce aerosols that contain the basic oxides $K_2O$, $Na_2O$, and CaO. The influence of these oxides on pH will depend on the amount that has entered the water pool, the initial pH and buffering capacity of the solution, the quantity of

**Table 3.1 Materials that affect pH in containment water pools**

- Boron oxides (acidic)
- Basic fission product compounds such as cesium hydroxide or cesium borates (basic)
- Iodine as HI (acidic)
- pH additives (basic)
- Atmospheric species such as carbon dioxide or nitric acid (acidic)
- Core-concrete aerosols (basic)
- Pyrolysis and radiolysis products from organic materials (acidic)

water, and the extent of dissolution of the aerosol material. One of the TRENDS models calculates the pH in water pools.

### 3.2.2 Nitric Acid Formation and pH Control

Water that is exposed to air absorbs $CO_2$ to form carbonic acid, which lowers pH. The pH of water approaches a limiting value of ~5.65 due to this process. In addition, nitric acid can be produced by the irradiation of water and air. Table 3.2 shows the relationship between the formation of nitrate ions and hydrogen ions from the irradiation of an air-water system. Table 3.3 shows the decrease in pH for an irradiated solution that contained trisodium phosphate with an initial pH of 9.0. During the irradiation, nitric acid and atmospheric $CO_2$ decreased the pH as shown. Phosphate solutions have their maximum pH buffer capacity at a pH near 7. This buffer capacity is reflected here in the length of time that the pH remained near 6.5. Once the buffer capacity was exceeded, the pH continually decreased.

Because of $CO_2$ and nitric acid, the pH is not likely to remain at some preadjusted value. A buffer system to retard changes from the desired pH is expected to provide a more stable pH level.

Two different buffer systems could be used in containment water pools: a phosphate buffer and a borate buffer. The phosphate buffer has a maximum capacity near pH 7, while the borate buffer has its maximum capacity near pH 9. Buffer capacity is often evaluated in terms of its buffer value $B$, which is defined by

$$B \equiv \frac{db}{dpH}$$

where $db$ is an increment of strong base in mol/L. With the addition of strong acids, a negative increment $-db$ is used. Bates[21] has shown that the relationship between the maximum buffer value, $B_{max}$, and concentration of a buffer, $C$, can be written as:

$$B_{max} = 0.576\ C$$

Thus, a given concentration of phosphate would have the same buffer value at a pH near 7 that the same concentration of borate would have at a pH near 9. The selection of the buffer system is important in determining the pH to be maintained. From a strictly chemical standpoint, selecting a borate for the buffer to maintain a pH near 9 is just as simple as selecting a phosphate to maintain a pH near 7.

**Table 3.2 Concentrations of $H^+$ and $NO_3^-$ in water due to irradiation***

| Irradiation time (h) | $[H^+]$ from pH | $[NO_3^-]$ from ion electrode |
|---|---|---|
| 6 | $3.2 \times 10^{-5}$ | $6.5 \times 10^{-5}$ |
| 12 | $6.3 \times 10^{-5}$ | $6.7 \times 10^{-5}$ |
| 22 | $1.0 \times 10^{-4}$ | $1.0 \times 10^{-4}$ |
| 65 | $2.5 \times 10^{-4}$ | $1.8 \times 10^{-4}$ |
| 114 | $5.0 \times 10^{-4}$ | $4.0 \times 10^{-4}$ |

*100 mL in closed 200-mL container at rate of 0.6 Mrad/h.

**Table 3.3 Effects of irrradiation dose* on pH in trisodium phosphate solution**

| Time (h) | pH |
|---|---|
| 0 | 9.0 |
| 4 | 6.4 |
| 7 | 6.5 |
| 23 | 6.5 |
| 41 | 4.7 |
| 63 | 3.9 |

*Dose rate, 0.53 Mrad/h.

Recently, a patent was issued for a method of pH control and gettering of iodine species which employs well-dispersed silver carbonate.[22]

## 3.3 Processes That Alter the Chemical Forms of Iodine in Containment

### 3.3.1 Radiolysis

#### 3.3.1.1 Description of Calculated Model

In the presence of radiation, the equilibrium formation of $I_2$ from $I^-$ is strongly dependent on pH and weakly on temperature and concentration. Ignoring the last two effects,[4] this dependence can be written as

$$F(pH) = \textit{equilibrium fraction} = \frac{[I_2]}{[I_2] + [I^-]} \qquad (18)$$

where [x] is the concentration of $I_2$ or $I^-$ (g-atom/L). Data from Lin,[23] as shown in Figure 3.1, illustrate this effect for several initial concentrations and pH values using solutions that were at ambient temperature and had been irradiated for 1 h at 4.5 Mrad/h. The final pH values were not indicated but probably decreased slightly since no mention is made of buffering in the experiment. The values of pH >6 may not be quantitatively useful since the very small conversion fractions are probably incorrect due to measurement error. As seen in Figure 3.1, $F$ is near 0 for pH >7 and near 1 for pH <2 but experiences a drastic change in the

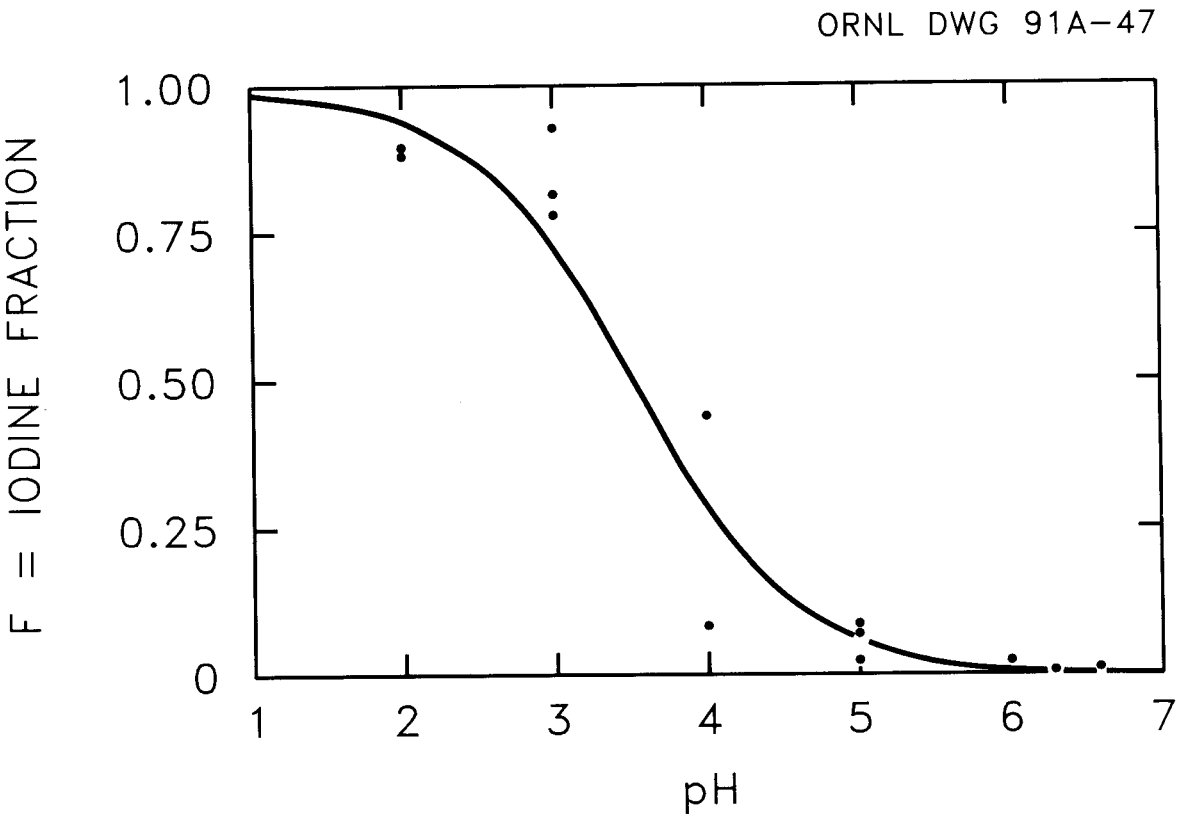


**Figure 3.1** Radiolytic conversion of $I^-$ to $I_2$ [data from C. C. Lin, *J. Inorg. Nucl. Chem.* 42, 1101 (1980)]

range 3 < pH < 4. As discussed in Appendix C, this can be effectively modeled by the functional form

$$F = [1 + e^{\alpha\,\mathrm{pH} + \beta}]^{-1} \qquad (19)$$

Equation 19 was fit to Lin's data by minimizing the sum of least-squares residuals, which yields

$$\alpha = 1.72 \qquad \beta = -6.08 \qquad (20)$$

Similar data are given by Naritami et al.[24] for $5 \le \mathrm{pH} \le 9$. They subjected borated $I^-$ solutions of $10^{-4}$, $10^{-5}$, and $10^{-6}$ mol/L to much lower dose rates ($^{60}$Co gamma rays of 0.1 Mrad/h) for 1 h. The model of Equations 19 and 20 gives a good match to these data for concentrations of $10^{-4}$ mol/L, although the model overestimates conversion for the lower concentrations.

If the pH is maintained sufficiently high through buffering or addition of sufficient basic material, very little conversion will occur. In this case, most iodine remains dissolved as $I^-$. Lin's data generally indicate <1% conversion at pH = 7. This value declines as the total iodine concentration decreases. The data of Naritomi show a conversion of 0.2% for iodide concentrations of $10^{-4}$ mol/L and 0.01% at lower concentrations. Data measured for this study indicate that for a dose rate of 0.35 Mrad/h, an iodine concentration of $10^{-4}$ mol/L conversion was 0.003% after 4 h irradiation and 0.03% after 24 h. The last value, 0.03%, has been used in the present work.

If the pH level is not deliberately controlled, it may decrease sufficiently to allow considerable conversion of $I^-$ to $I_2$. The primary mechanism is radiolytic generation of nitric acid (see Section 3.2.2). If the pH is neutral initially, then this effect soon dominates, resulting in

$$[H^+] = 10^4\, g(HNO_3)\, \frac{E_{dep}}{V_L N_a} \qquad (21)$$

where

$[H^+]$ = concentration of $H^+$ (mol/L),
$g(HNO_3)$ = rate of $HNO_3$ production due to irradiation (molecules/100 eV),
$E_{dep}$ = total energy deposition due to fission product decay (MeV),
$V_L$ = volume of water (L),
$N_a$ = $6.022 \times 10^{23}$ (molecules/mol).

The data in Table 3.2 indicate that at 30°C (86°F)

$$g(HNO_3) = 0.007\ molecules/100\ eV \qquad (22)$$

This relationship is based on radiation absorption by the aqueous phase. The actual mechanism for the formation of nitric acid is not known. It may occur in the aqueous phase, in the gas phase, or at the gas-surface interface. The containment water volume, $V_L$, is usually constant over the period during and subsequent to significant fission product releases.

The energy deposition over a time $\Delta t$ is

$$E_{dep} = \dot{E}_{dep}\, \Delta t = \Delta t \sum m_j\, \dot{e}_j \qquad (23)$$

where

$\Delta t$ = time (h),
$\dot{E}_{dep}$ = total energy deposition rate (MeV/h),
$m_j$ = mass of nuclide group $j$ in pool (g),
$\dot{e}_j$ = energy deposition rate per unit mass of nuclide group $j$ (MeV/h·g).

Various groupings of fission products and actinides have been considered in past safety studies. A grouping compatible with that used in STCP accident studies was selected for this study (see Table 3.4). The specific energy deposition rate $\dot{e}_j$ for each group depends on the relative distribution of radioactive nuclides, which, in turn, depends on such factors as fuel enrichment, power history, and additives or other materials in the fuel or reactor.

A detailed analysis of Browns Ferry (a large BWR with Mark I containment) accident sequences has been performed by ORNL staff members. Using the ORIGEN2 code,[25] nuclide inventories were determined for the highest and lowest power of each type of fuel

Table 3.4 Nuclide groupings and group-specific energy deposition rates

| Group index, j | Characteristic element | Included nuclides | Energy deposition rate, $\dot{e}_j \times 10^{-19}$ (MeV/h·kg) |
|---|---|---|---|
| 1 | I | I, Br | 425.0 |
| 2 | Cs | Cs, Rb | 3.971 |
| 3 | Te | Te, Se, Sb | 20.06 |
| 4 | Sr | Sr | 31.25 |
| 5 | Ba | Ba | 8.900 |
| 6 | Ru | Ru, Tc, Rh, Mo, Pd | 6.613 |
| 7 | Ce | Ce, Pu, Np | 1.540 |
| 8 | La | La, Am, Cm, Y, Pr, Nd, Pm, Sm, Eu, Zr,* Nb | 25.46 |
| 9 | Xe | Xe, Kr | 2.902 |

*Includes only fission products.

assembly in the cycle 6 fuel loading. Nuclide inventories for every assembly in the reactor were then determined by interpolation based on power history, using the high and low cases for that assembly type. These inventories were subsequently combined to obtain a total core inventory for every fission product nuclide of significance either in mass or decay energy at 5 h after shutdown. Assuming all decay energy is absorbed, the total inventories were used with decay energy data for each nuclide to obtain energy deposition rates $\dot{e}_j$ for each fission product group, which are also shown in Table 3.4. Complete details of this calculation can be found in Reference 26.

The group energy deposition rates for the Browns Ferry BWR are applied to all sequences considered in the present study. This is a very legitimate assumption for the Peach Bottom plant, which is also a BWR-Mark I nearly identical to Browns Ferry in size and design. A similar assumption is also made for Grand Gulf, also a BWR. These assumptions are analogous to those made in previous reports[1,2] using ORNL calculations for the Browns Ferry cycle 4 loading. While PWRs have many characteristics different from BWRs, the fission process results in the same distribution of fission products. Although the final distribution is somewhat affected by geometry and additives, the group energy deposition rates are assumed to be sufficiently similar to BWR values to permit use of the values in Table 3.4 for Sequoyah and Surry sequences.

### 3.3.1.2 Mass Manipulations

The group masses $m_j$ are obtained by multiplying the total core inventory $\bar{m}_j$ by the estimated fractional release into containment

$$m_j = f_j \, \bar{m}_j \tag{24}$$

Total core inventories for the plants are those identified in previous reports[1,2] and are given in Appendix D. Various estimates of the fractional releases $f_j$ can be obtained from Nourbakhsh.[27] He has compiled results from many STCP accident calculations (including those mentioned in this study) and has stated bounding estimates for the fractions of core inventory released into containment due to the following effects:

(1) release from RCS prior to vessel failure
(2) release at vessel breach
(3) ex-vessel release due primarily to core-concrete interactions

(4) late revolatilization from the RCS.

Categories 1, 2, and 4 can be combined to yield a total release into the containment from the primary system. The release fractions adopted from Nourbakhsh and used in this study are shown in Table D.2 of Appendix D.

Finally, $\Delta t$ in Equation 23 is the time needed to reach the approximate steady state. In general, the first phase of an accident can be considered to reach steady state in 10 to 15 h (see Section 3.1), and this is the time range considered for $\Delta t$. The pH can be calculated from

$$pH = -\log_{10} [H^+] = -\ln [H^+]/\ln 10$$

and the fractional conversion in Equation 18 then takes the form

$$F = \left[1 + e^{b}[H^+]^{-\frac{a}{\ln 10}}\right]^{-1} = \left[1 + 5.55 \times 10^{13} \left(\frac{V_L}{E_{dep}}\right)^{0.747}\right]^{-1} \quad (25)$$

Thus, when pH is not controlled, fractional conversion is directly dependent on the liquid volume $V_L$ in which radiolysis occurs; the energy deposition $E_{dep}$, which itself depends on the amounts of radioactive species in water; and the time $\Delta t$ allowed for the radiolysis process to reach steady-state conditions.

### 3.3.1.3 Gas-Liquid Partitioning

The equilibrium distribution of a single volatile species, such as $I_2$, is represented by the partition coefficient

$$P = \frac{[I_2\ (aq)]_{eq}}{[I_2\ (g)]_{eq}} \quad (26)$$

This quantity is inversely related to the Henry's Law constant $K$ (i.e., $P = 1/K$) and should not be confused with the overall iodine partition coefficients often used in reactor safety studies. Partition coefficients for $I_2$ were calculated from

$$\log_{10} P = 6.29 - 0.0149\ T \quad (27)$$
$$T\ (K)$$

This relationship gives the experimental value reported by Eguchi et al.[28] and by Sanemasa et al.[29] at 298 K (77°F). Extrapolation of the experimental results of these investigators to 373 K (212°F) yielded a partition coefficient of 3. Furrer et al.[30] reported a calculated partition coefficient at 373 K (212°F) of 9.

Some of the data used in this calculation was based on estimated parameters. Equation 27 gives a partition coefficient of 5.3 at 373 K (212°F), the approximate average of the calculated value, and the extrapolation of the measured values.

While it may take considerable time to approach such equilibration in a large system such as a reactor containment, Equation 26 can still be used to estimate $I_2$ volatility. In fact, instant equilibration is a conservative assumption since considerable holdup could be expected in real-life situations. A rigorous analysis would consider the delay associated with the evaporation of volatile species from water pools. This phenomenon is not well understood, and only crude models are available. Thus, the escape of $I_2$ from water pools will be modeled by assuming that Equation 26 holds continuously as $I_2$ is produced radiolytically.

### 3.3.1.4 Gas-Phase Reactions: Formation of Organic Iodides

The process of converting $I_2$ into organic iodides (chiefly $CH_3I$) is still not fully understood. Postma and Zavodoski[31] reviewed production rates from about 70 containment tests and determined that the asymptotic steady-state conversion to $CH_3I$ was

$$percent\ I_2\ converted = 0.19\ C_{mo}^{-0.26}\ , \quad (28)$$

where $C_{mo}$ = initial $I_2$ concentration (mg/m$^3$). This equation was based on 69 containment experiments. In a more recent review, Beahm et al.[5] described formation using the rate equation

$$\frac{dC_o}{dt} = \alpha(C^* - C_o) \qquad (29)$$

where

$\alpha$ = formation rate constant ($s^{-1}$),
$C_o$ = organic iodide concentration (mg iodine/$m^3$),
$C^*$ = steady-state organic iodide concentration (mg iodine/$m^3$).

They assigned the constant value $\alpha = 0.0051$ based on empirical evidence and used

$$C^* = 0.0189\ C_{mo}^{0.82} \qquad (30)$$

in place of Equation 28. This equation was based on containment experiments performed with irradiated fuel rather than simulated materials. The percent conversion to organic iodide when irradiated fuel was used was somewhat greater than that obtained from simulant materials (cf. Figure 4, Reference 5).

By converting units to g-atom/L, Equation 30 can be rewritten as

$$[CH_3I] = \beta\ [I_2]^{0.82} \qquad (31)$$

where $\beta = 0.0189\ (10^6 \cdot MW)^{-0.18}$, MW being the molecular weight of I. For MW = 130, then $\beta = 6.55 \times 10^{-4}$, which indicates that generally <1% of gaseous iodine will be organic.

### 3.3.1.5 Overall Behavior

As described in the previous sections, the distribution of species throughout the gas and liquid phases can be estimated from models for three basic processes: radiolytic conversion of $I^-$ to $I_2$ in water, evaporation of $I_2$, and gas-phase formation of organic iodides. Defining the desired quantities as concentration variables (g-atom/L)

$$C_1 = [I_2\ (aq)],\ C_2 = [I_2\ (g)],\ C_3 = [I^-\ (aq)],\ C_4 = [CH_3I\ (g)]$$

Equations 26, 18, and 31 can be rewritten as

$$C_1 = PC_2 \qquad (32a)$$

$$C_3 = \frac{(1 - F)}{F}\ C_1 \qquad (32b)$$

$$C_4 = \beta\ C_2^{0.82} \qquad (32c)$$

In addition, the total iodine inventory $N_T$ (g-atom) is equal to the initial $I^-$ entering the containment and remains constant throughout the distribution process:

$$N_T = V_L\ (C_1 + C_3) + V_g\ (C_2 + C_4) \qquad (32d)$$

There are four equations (Eqs. 32a—32d) and four unknowns ($C_1$, $C_2$, $C_3$, and $C_4$); all equations except Equation 32c are linear, and its nonlinearities are very mild.

To obtain solutions to the system, Equations 32a—32c are substituted into Equation 32d, yielding

$$N_T = \frac{V_L}{F}\ PC_2 + V_g\ (C_2 + \beta C_2^{0.82}) \qquad (33)$$

which can be arranged into the form

$$C_2 = \frac{\left(N_T - V_g\ \beta C_2^{0.82}\right)}{\left(\frac{PV_L}{F} + V_g\right)} \qquad (34)$$

This represents a convenient form for fixed-point iteration, which usually converges to a relative error of $10^{-4}$ within three to five iterations. Once $C_2$ has been determined from Equation 34, the other concentrations are obtained from Equations 32a—32c.

Because organic iodide is such a small part of the total, it is helpful to examine the distribution behavior without considering organic iodide. By ignoring Equation 32c, Equation 33 becomes

$$N_T = \frac{V_L}{F} PC_2 + V_g C_2$$

which can be rearranged to obtain

$$\frac{N_2}{N_T} = \left(1 + \frac{V_L P}{V_g F}\right)^{-1} \qquad (35)$$

where $N_2 = V_g C_2$ = g-atom of $I_2$ in gas. Equation 35 is a convenient expression of the fraction of iodine that is volatilized. (Consideration of organic iodide will increase this fraction very slightly.) For the case of uncontrolled pH, substitution of Equation 25 into Equation 35 yields

$$\frac{N_2}{N_T} = \left\{1 + \frac{V_L P}{V_g}\left[1 + 5.55 \times 10^{13}\left(\frac{V_L}{E_{dep}}\right)^{0.747}\right]\right\}^{-1} \qquad (36)$$

which is an expression for the fraction of volatile iodine (as $I_2$). To use Equation 35 or 36, it is necessary to estimate the characteristics or approximate values for each of the following quantities:

$V_L$, $V_g$ = liquid and gas volumes (L),
$T$ = air-water interface temperature (which permits computation of the partition coefficient $P$ by Equation 27).

For the case of uncontrolled pH, it is also necessary to obtain

$m_i$ = masses of fission products in the containment (from which the dose term $E_{dep}$ is calculated by Equation 24),
$\Delta t$ = approximate duration of the radiolysis phase(s) in category 1 (see Section 3.1).

If Equation 35 or 36 is used instead of solving the nonlinear Equation 34, then a good approximation to the airborne organic iodide inventory can be obtained by simply using Equation 32c. Furthermore, Equations 35 and 36 are in particularly convenient form not only to estimate iodine volatility, but also to estimate the individual phenomena and their impact on overall behavior.

### 3.3.2 Results of Iodine Behavior in Containment

The analysis described in Section 3.3.1 has been applied to each of the seven accident sequences listed in Table 1.1. Using whole core inventories from previous reports,[1,2] the release fractions of Nourbakhsh[27] (including both vessel and core-concrete releases), and the nuclide group energy deposition rates in Table 3.4, the energy deposition rate $\dot{E}_{dep}$ can be calculated for each plant using Equations 23 and 24. The results are shown in Appendix E.

Once the energy deposition has been computed, the remaining quantities can be calculated by solving the system of equations 32. Liquid and gas volumes and temperatures were obtained from sequence documentation.[1,2] The gas volumes used for BWRs include all primary containment space, although it may sometimes be appropriate to use only wetwell airspace, depending on sequence considerations. Partition coefficients were calculated as functions of temperature from Equation 27. The total iodine inventory initially deposited in water as $I^-$ was calculated using previously mentioned mass inventories and release fractions and assuming a molecular weight of 130.

These various data and the quantities calculated from them are listed for each accident sequence in Table 3.5. From the table, it appears that PWRs exhibit dose rates considerably higher than do BWRs, contributing to the much higher conversion fractions. The presence of extremely large water volumes is a distinct advantage for BWRs in this regard. The conversion data of Lin[23] were taken at a dose rate of 4.5 Mrad/h in the range of PWR rates. The data taken at ORNL are generally in the range of BWR dose rates (i.e., 0.35 to 0.6 Mrad/h). Both sets of data indicate that conversion is dominated by pH effects. In this study, two scenarios were evaluated: (1) control of pH above 7 and (2) uncontrolled pH with resulting drops below 7 due to nitric acid. For

Table 3.5 Data for equilibrium analysis of example sequences

| Plant | Accident | Volume ($m^3$) Liquid | Volume ($m^3$) Gas | Temperature (°C) | Partition coefficient | $\dot{E}_{dep}$ (MeV/h)* $\times 10^{-23}$ | Dose rate** (Mrad/h) | Total I (g-mol) | Aqueous $I_2$ (%)† $\Delta t = 10$ h | Aqueous $I_2$ (%)† $\Delta t = 15$ h |
|---|---|---|---|---|---|---|---|---|---|---|
| Grand | TCγ | 4550 | 39650 | 102 | 5.0 | 1.2778 | 0.45 | 122.5 | 14 | 18 |
| Gulf | TQUVγ | 5171 | 39650 | 60 | 21.2 | 1.3020 | 0.40 | 136.2 | 13 | 18 |
| Peach | AEγ | 4000 | 7873 | 54 | 26.0 | 1.2223 | 0.49 | 127.7 | 16 | 21 |
| Bottom | TC2 | 4500 | 7873 | 118 | 2.9 | 1.1997 | 0.43 | 114.9 | 14 | 19 |
| Sequoyah | TBA | 1465 | 36404 | 112 | 3.6 | 0.9267 | 1.01 | 105.2 | 24 | 30 |
| Surry | TMLB′ | 115 | 51000 | 93 | 6.8 | 0.5136 | 7.16 | 57.2 | 59 | 67 |
| | AB | 172 | 51000 | 112 | 3.6 | 0.6912 | 6.44 | 85.8 | 58 | 66 |

*Calculated from Equation 23.
**Calculated from the expression: dose rate (Mrad/h) = $1.60219 \times 10^{-20} \dot{E}_{dep}/(\rho V_L)$, where $\rho = 1$ kg/L is assumed.
†Calculated from Equation 19.

this calculation, it was not necessary to specify the material that was used to control the pH at 7 or above.

If the pH is controlled so that it stays above 7, a reasonable value for the fraction of $I^-$ converted to $I_2$ is $3 \times 10^{-4}$ (Section 3.3.1.1). Using this and the other computed quantities in Table 3.5, the system of equations 32 is solved to yield the species distributions in Table 3.6. It should be noted that data in Tables 3.5 and 3.6 refer to the total iodine in containment, not the core inventory of iodine. Table 3.6 indicates a small production of volatiles for PWRs but virtually none for BWRs.

Such results are strongly dependent on the aqueous conversion fraction of $F = 3 \times 10^{-4}$, which represents a best estimate of the maximum from ORNL data. Thus, if pH is maintained at 7 or above, only a small additional amount of $I_2$ is expected in the gas phase in PWR systems.

If the pH falls below 7, a system for conrolling pH is not being used and the decreased pH results in a larger fraction of aqueous $I^-$ being converted to $I_2$. Evaporation of this volatile species so as to maintain equilibrium partitioning will result in greater atmospheric $I_2$. This, in turn, yields higher organic iodide concentrations. The aqueous conversion fraction itself is determined from Equation 25, which requires a value for the equilibration time $\Delta t$. As discussed in Section 3.3.1, a value of $\Delta t = 15$ h is appropriate and yields the results shown in Table 3.7 for the equilibrium species distributions. As expected, the levels of airborne volatiles are much higher than in the controlled case, indicating almost complete conversion for PWRs.

The gaseous $I_2$ fraction is considerably higher in PWRs than in BWRs because the large water volumes in the latter both lower the dose rate and retain greater quantities of dissolved $I_2$. This last effect also depends on the gas volume and the ratio of gas to liquid volumes. It is ironic that the relatively small gas space in the Peach Bottom reactor (generally a safety liability) permits noticeably less evaporation than other reactors, resulting in the lowest gaseous $I_2$ fractions.

The other principal effect is due to temperature — the $I_2$ partition coefficient changes markedly over the range of temperatures used. This is most noticeable in the BWR sequences where different sequences at the same plant show large differences in the airborne $I_2$ fraction. Thus, an increase in containment temperature (at the gas-liquid interface) from 60 to 115°C (140 to 239°F) produces nearly an order of magnitude increase in the airborne fraction.

The organic iodide is present in PWRs at about 0.5% of core inventory; in BWRs, this concentration is closer to 0.1%. The $I_2$ generated by the radiolytic conversion of $I^-$ dominates the amount released as $I_2$ from the RCS. Further, based on the equilibrium assumption, the presence of some $I_2$ already airborne will result in less evaporation of $I_2$ formed radiolytically. Hence, for the case of uncontrolled pH, the cumulative total is well represented by the equilibrium amount formed within containment.

### 3.3.3 Evaporation to Dryness

Water pools or condensate puddles may evaporate in containment and provide a mechanism for the release of dissolved aqueous iodine to the gas. As with all processes involving aqueous iodine, the extent of volatile iodine produced is related to pH. Table 3.8 gives percentages of volatile iodine produced when $1 \times 10^{-4}$ mol/L CsI solutions were evaporated to dryness at 95°C. Radiation increased the percentage of volatile iodine by about an order of magnitude. In solutions where the initial pH was 7 or below, there was a rapid decrease in pH just before dryness.

The overall impact of evaporation to dryness will depend on the extent to which it occurs in containment.

Table 3.6 Distribution of iodine species for pH controlled above 7

| Plant | Accident | Fraction of total iodine in containment (%) | | | |
|---|---|---|---|---|---|
| | | $I_2$ (g) | $I_2$ ($\ell$) | $I^-$ ($\ell$) | $CH_3I$ (g) |
| Grand Gulf | TC $\gamma$ | 0.05 | 0.03 | 99.92 | 0.001 |
| | TQUV $\gamma$ | 0.01 | 0.03 | 99.96 | 0.0003 |
| Peach Bottom | AE $\gamma$ | 0.002 | 0.03 | 99.97 | 0.0001 |
| | TC2 $\gamma$ | 0.02 | 0.03 | 99.95 | 0.0004 |
| Sequoyah | TBA | 0.21 | 0.03 | 99.76 | 0.004 |
| Surry | TMLB′ $\gamma$ | 1.9 | 0.03 | 98.0 | 0.03 |
| | AB $\gamma$ | 2.4 | 0.03 | 97.5 | 0.03 |

Table 3.7 Distribution of iodine species for uncontrolled pH

| Plant | Accident | Fraction of total iodine in containment (%) | | | |
|---|---|---|---|---|---|
| | | $I_2$ (g) | $I_2$ (ℓ) | $I^-$ (ℓ) | $CH_3I$ (g) |
| Grand Gulf | TC γ | 26.6 | 15.3 | 58.0 | 0.2 |
| | TQUV γ | 6.6 | 18.3 | 75.1 | 0.06 |
| Peach Bottom | AE γ | 1.6 | 21.6 | 76.8 | 0.01 |
| | TC2 γ | 10.9 | 18.0 | 71.0 | 0.07 |
| Sequoyah | TBA | 69.2 | 9.9 | 20.5 | 0.4 |
| Surry | TMLB′ γ | 97.1 | 1.5 | 0.7 | 0.7 |
| | AB γ | 97.6 | 1.2 | 0.6 | 0.6 |

Table 3.8 Iodine volatility of $1 \times 10^{-4}$ mol/L CsI solutions during evaporation to dryness

| Test conditions | | Percent volatile | | |
|---|---|---|---|---|
| Initial pH | Borate (*M*) | Without radiation | With radiation (total dose, 2.1 MR) | Final pH just before dryness |
| 4.4 | 0.2 | 7.2 | >99 | 1.8 to 2.0 |
| 4.4 | 0* | 2.0 | | 3.6 |
| 6.0 | 0.2 | 6.8 | 55 | 2.0 to 2.2 |
| 7.0 | 0.2 | | 32 | 3.0 |
| Pure water | 0 | 1.6 | 21 | |
| 9.0 | 0.2 | 1.8 | 22 | 8.5 |

*Phosphoric acid added to adjust the pH to 4.4.

# 4 Technical Findings

## 4.1 Perspective and Scope of Study

This study assumed that iodine forms in containment can be delimited by an examination of the seven severe accident sequences in LWR plants, along with an evaluation of associated processes. The associated processes include the deposition of CsOH on RCS surfaces and the effects of radiolysis. The issue is the chemical form of iodine that may be produced in the RCS and in containment — not the ultimate disposition of the various chemical forms. For example, it is likely that much of the gaseous $I_2$ in containment would be removed by engineered safety features or would deposit on painted or metal surfaces.

## 4.2 Assessment of Iodine Chemical Forms in the RCS

The maximum iodine as I plus HI calculated for the seven severe accident sequences is 3.2%. Iodine in all forms other than I, HI, and CsI is estimated to be less than 1%. Although this analysis only considered seven sequences at four plants, it is reasonable to consider that a maximum of 5% of the iodine would be present as elemental iodine and HI for all accident sequences. A minimum value would not be expected to be less than 1%. The remaining 95% of the iodine would be as CsI.

The gaseous forms of iodine that entered containment from the RCS were given in terms of both elemental iodine and HI. There is a fundamental reason for this. The two forms of iodine are related by

$$I + \frac{1}{2}H_2 \rightleftharpoons HI \qquad (37)$$

In the temperature range of 1000 to 2000 K, thermochemical data for this reaction were fit to give

$$\frac{P_{HI}}{P_I} = (P_{H_2})^{-1/2} \cdot \exp\left(\frac{1.024 \times 10^4}{T} - 5.645\right) \qquad (38)$$

Lower temperatures and higher hydrogen pressures tend to favor HI over I, with the opposite conditions favoring I over HI. Five percent of iodine as I plus HI, with not less than 1% in either form, means that the $P_{HI}$-to-$P_I$ ratio in Equation 38 would range from 0.25 to 4. With a hydrogen pressure of 1 atm, this would occur in the temperature range of 1456 to 2404 K (2161 to 3868°F); with a hydrogen pressure of 10 atm, it would occur in the temperature range of 1251 to 1893 K (1792 to 2948°F). These conditions are reasonable for situations that lead to the formation of I or HI.

The major uncertainty is the extent to which CsOH will react with oxide materials and reduce its vapor pressure. If the reaction of CsOH is to have a major impact on the iodine chemical forms, most of it (certainly more than 90%) must be fixed at a very low vapor pressure.

## 4.3 Assessment of Iodine Chemical Forms in Containment

The production of $I_2$ in containment will be directly related to the pH levels of the water pools. As illustrated in Figure 4.1, failure to control the pH at or above 7 could result in an increase of $I_2$ in the atmosphere of between 4,100 and 33,000% as compared with the case where pH is controlled for PWRs. Essentially all of the $I_2$ could become gaseous in the PWRs without pH control. For BWRs, the increase is between 53,000 and 80,000%, with about 25% of the $I_2$ becoming gaseous. The dramatic difference in the amount of $I_2$ between the cases where pH was uncontrolled below 7 and the controlled cases speak for themselves. A major uncertainty is the extent of evaporation to dryness. From 2 to 20% of the iodine in water pools that have evaporated could be converted to a volatile form, most likely as $I_2$.

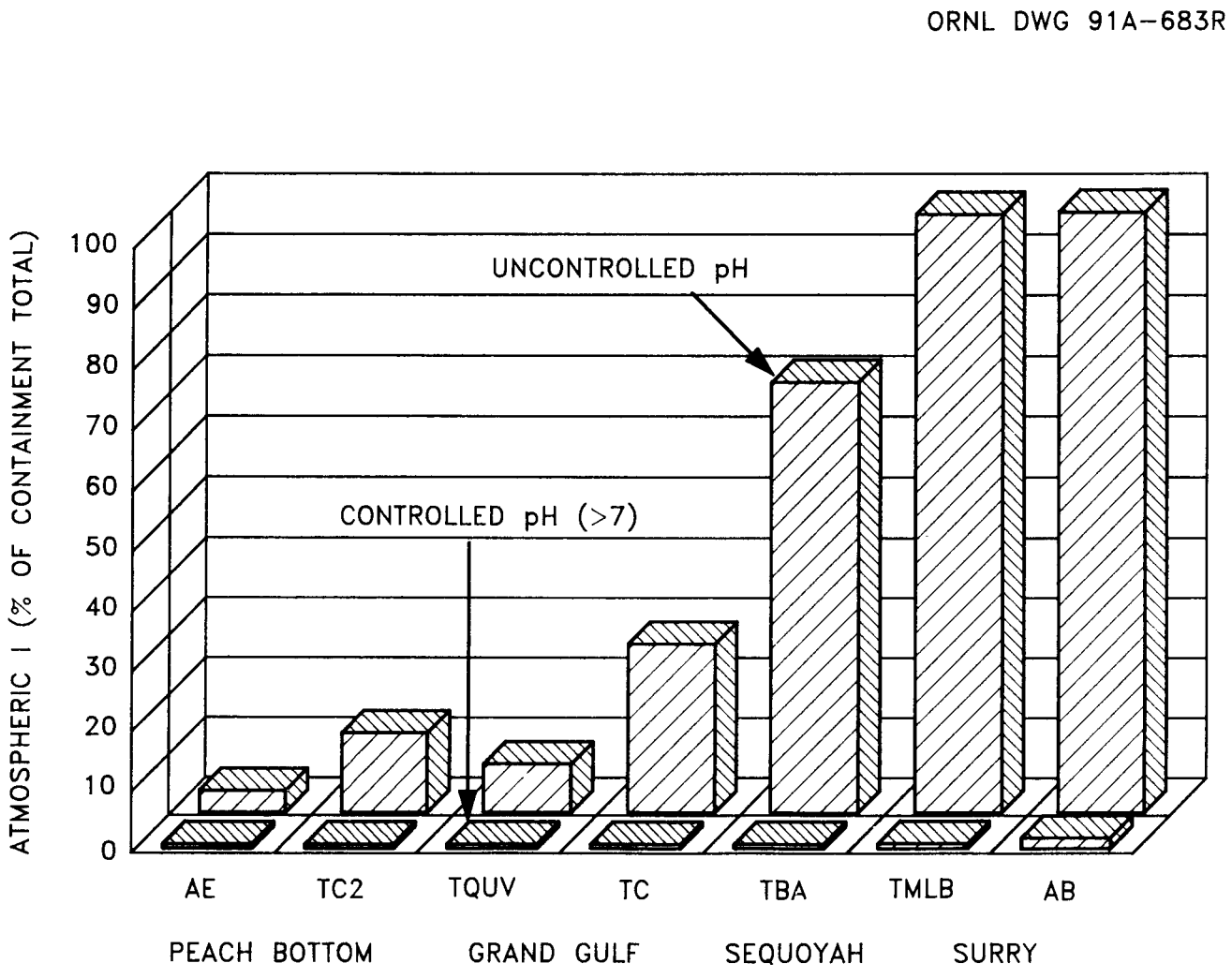


**Figure 4.1 Additional atmospheric elemental iodine released**

# 5 References


1. Gieseke, J. A. et al., "Radionuclide Release Under Specific LWR Accident Conditions," BMI-2104, Battelle Columbus Laboratories, 1984.

2. Denning, R. S. et al., "Radionuclide Release Calculations for Selected Severe Accident Scenarios," NUREG/CR-4624 (BMI-2139), Battelle Columbus Laboratories, 1986.

3. FACT, a copyrighted product of THERMFACT Ltd., 447 Berwich Ave., Mount-Royal, Quebec, Canada, H3R 1Z8.

4. Wisby, S. J. et al., "Iodine Behavior in Containment Under LWR Accident Conditions," pp. 6—29 in *Proceedings of the Symposium on Chemical Phenomena Associated with Radioactivity Releases During Severe Nuclear Plant Accidents*, Anaheim, Calif., September 1986.

5. Beahm, E. C., W. E. Shockley, and O. L. Culberson, "Organic Iodide Formation Following Nuclear Reactor Accidents," NUREG/CR-4327, Oak Ridge National Laboratory, 1985.

6. Lemire, R. J. et al. "Assessment of Iodine Behavior in Reactor Containment Buildings from a Chemical Perspective," AECL-6812, 1981.

7. Burns, W. G. et al., "The Radiolysis of Aqueous Solutions of Caesium Iodide and Caesium Iodate," AERE-R-13520, 1990.

8. U.S. Nuclear Regulatory Commission, Regulatory Guide 1.3, "Assumptions Used for Evaluating the Potential Radiological Consequences of a Loss-of-Coolant Accident for Boiling Water Reactors," June 1974.

9. U.S. Nuclear Regulatory Commission, Regulation Guide 1.4, "Assumptions Used for Evaluating the Potential Radiological Consequences of a Loss-of-Coolant Accident for Pressurized Water Reactors," June 1974.

10. Wooten, R. O., P. Cybulskis, and S. F. Quayle, "MARCH2 Meltdown Accident Response Characteristic Code Description and User's Manual," NUREG/CR-3988 (BMI-2115), Battelle Columbus Laboratories, 1984.

11. Jordan, H. and M. R. Kuhlman, "TRAP-MELT User's Manual," NUREG/CR-4205 (BMI-2124), Battelle Columbus Laboratories, 1985.

12. Chance, E. M. et al., "FACSIMILE: A Computer Program for Flow and Chemistry Simulation, and General Initial Value Problems," AERE-R-8775, AERE Harwell, December 1977.

13. Johnson, I. et al., "Downstream Behavior of Volatile Iodine, Cesium, and Tellurium Fission Products," EPRI NP-6182, January 1989.

14. Silberberg, M. et al., "Reassessment of Technical Bases for Estimating Source Terms," NUREG-0956, U.S. Nuclear Regulatory Commission, July 1986.

15. Megaw, W. J. and F. G. May, "The Behavior of Iodine Released in Reactor Containers," *J. Nucl. Energy, Pts. A/B*, **16**, 427 (1962).

16. Croft, J. F. and R. S. Isles, "Experimental Release of Radioiodine in the Zenith Reactor Containment," AEEW-R-172, 1962.

17. Parker, G. W., G. E. Creek, and W. J. Martin, "Fission Product Transport and Behavior in the Stainless Steel-Lined Containment Research Installation," ORNL-4502, 1971.

18. Hilliard, R. K. and L. F. Coleman, "Natural Transport Effects on Fission Product Behavior in the Containment Systems Experiment," BNWL-1457, 1970.

19. Cline, J. E. et al., "Measurements of $^{129}I$ and Radioactive Particulate Concentrations in the TMI-2 Containment Atmosphere During and After the Venting," GEND-009, April 1981.

20. Lillian, D. et al., *Environ. Sci. Technol.* **12**, 1042 (1975).

21. Bates, R. G., *Determination of pH*, p. 99, Wiley, New York, 1964.

22. Beahm, E. C. and W. E. Shockley, "Method for Gettering Organic, Inorganic, and Elemental Iodine in Aqueous Solutions," Patent ESID 518-X (April 1989).

23. Lin, C. C., "Chemical Effects of Gamma Radiation on Iodine in Aqueous Solutions," *J. Inorg. Nucl. Chem.* **42**, 1101 (1980).

24. Naritami, M. et al., "Batch-Type Tests on Formation of Volatile Iodine Species from Aqueous Iodide Solutions Under $^{60}Co$ $\gamma$-Ray Irradiation," *Proceedings of the Third CSNI Workshop on Iodine Chemistry in Reactor Safety*, Sept. 11-13, 1991, Toaki-mura, Japan.

25. Croff, A. G., "ORIGEN2 — A Revised and Updated Version of the Oak Ridge Isotope Generation and Depletion Code," ORNL-5621, Oak Ridge National Laboratory, July 1980.

26. Weber, C. F., "Calculation of Absorbed Doses to Water Pools in Severe Accident Sequences," ORNL/CSD/TM-274, Oak Ridge National Laboratory, 1991.

27. Nourbakhsh, H. P., "Estimate of Radionuclide Release Characteristics into Containment Under Severe Accident Conditions (Draft for Comment)," NUREG/CR-5747, Brookhaven National Laboratory, December 1991.

28. Eguchi, W., M. Adachi, and M. Yoneda, *J. Chem. Eng. Jpn.* **6**, 389 (1973).

29. Sanemasa, I. et al., *Bull. Chem. Soc. Jpn.* **57**, 1352 (1984).

30. Furrer, M., R. C. Cripps, and R. Gubler, *Nucl. Technol.* **70**, 290 (1985).

31. Postma, A. K. and R. V. Zavodoski, "Review of Organic Iodide Formation Under Accident Conditions in Water-Cooled Reactors," WASH-1233, U.S. Atomic Energy Commission, 1972.

32. Wren, D. J., "Kinetics of Iodine and Cesium Reactions in the CANDU Reactor Primary Heat Transport System Under Accident Conditions," AECL-7781, April 1983.

33. Frost, A. and B. Pearson, **Kinetics and Mechanism**, 2nd ed., p. 104, Wiley, New York, 1961.

34. Lorenz, K., H. Wagner, and R. Zellner, *Ber. Buns. Phys. Chem.* **83**, 556 (1979).

35. Kondrat'ev, V., *Kinetics of Chemical Gas Reactions*, AEC-tr-4493, 1958.

36. Chase, M. W., Jr. et al., *JANAF Thermochemical Tables*, 3rd ed., American Chemical Society, Washington, D.C., 1986.

37. Barin, I. and O. Knacke, *Thermochemical Properties of Inorganic Substances*, Springer-Verlag, Berlin, 1973.

# Appendix A. Data from Accident Sequence Calculations

Table A.1 Grand Gulf TC–MERGE output data from MARCH2

| Time (s) | Flow rate from core (lb/s) Hydrogen | Total | Core exit temperature (°F) | Pressure (psia) |
|---|---|---|---|---|
| 5381 | 0.0 | 0.543E+03 | 363 | 146 |
| 5498 | 0.0 | 0.591E+02 | 565 | 117 |
| 5504 | 0.319E-06 | 0.560E+02 | 578 | 117 |
| 5522 | 0.109E-05 | 0.480E+02 | 600 | 116 |
| 5552 | 0.656E-05 | 0.394E+02 | 641 | 115 |
| 5588 | 0.399E-04 | 0.333E+02 | 685 | 113 |
| 5612 | 0.112E-03 | 0.301E+02 | 710 | 112 |
| 5642 | 0.348E-03 | 0.270E+02 | 738 | 111 |
| 5678 | 0.110E-02 | 0.242E+02 | 768 | 110 |
| 5726 | 0.370E-02 | 0.208E+02 | 803 | 109 |
| 5756 | 0.669E-02 | 0.193E+02 | 825 | 108 |
| 5822 | 0.177E-01 | 0.138E+02 | 849 | 106 |
| 5858 | 0.181E-01 | 0.115E+02 | 851 | 105 |
| 5924 | 0.212E-01 | 0.996E+01 | 867 | 103 |
| 5978 | 0.251E-01 | 0.936E+01 | 884 | 102 |
| 6032 | 0.303E-01 | 0.884E+01 | 902 | 101 |
| 6080 | 0.360E-01 | 0.841E+01 | 920 | 100 |
| 6122 | 0.420E-01 | 0.822E+01 | 934 | 99 |
| 6182 | 0.525E-01 | 0.762E+01 | 963 | 98 |
| 6218 | 0.601E-01 | 0.724E+01 | 978 | 97 |
| 6284 | 0.772E-01 | 0.643E+01 | 1004 | 96 |
| 6326 | 0.901E-01 | 0.611E+01 | 1021 | 95 |
| 6380 | 0.110E+00 | 0.579E+01 | 1042 | 94 |
| 6446 | 0.139E+00 | 0.527E+01 | 1069 | 93 |
| 6512 | 0.172E+00 | 0.472E+01 | 1094 | 92 |
| 6578 | 0.212E+00 | 0.412E+01 | 1120 | 91 |
| 6647 | 0.251E+00 | 0.410E+01 | 1144 | 90 |
| 6691 | 0.270E+00 | 0.361E+01 | 1159 | 89 |
| 6742 | 0.301E+00 | 0.310E+01 | 1176 | 89 |
| 6836 | 0.302E+00 | 0.190E+01 | 1206 | 87 |
| 6911 | 0.308E+00 | 0.162E+01 | 1231 | 87 |
| 6974 | 0.320E+00 | 0.135E+01 | 1252 | 86 |
| 7075 | 0.308E+00 | 0.119E+01 | 1283 | 85 |
| 7126 | 0.300E+00 | 0.113E+01 | 1298 | 84 |
| 7176 | 0.294E+00 | 0.107E+01 | 1313 | 84 |
| 7252 | 0.286E+00 | 0.983E+00 | 1334 | 83 |
| 7327 | 0.280E+00 | 0.886E+00 | 1355 | 82 |
| 7390 | 0.274E+00 | 0.809E+00 | 1374 | 82 |
| 7478 | 0.269E+00 | 0.692E+00 | 1402 | 81 |
| 7617 | 0.257E+00 | 0.569E+00 | 1444 | 80 |

Table A.1 (Continued)

| Time (s) | Flow rate from core (lb/s) Hydrogen | Total | Core exit temperature (°F) | Pressure (psia) |
|---|---|---|---|---|
| 7705 | 0.245E+00 | 0.539E+00 | 1469 | 79 |
| 7831 | 0.230E+00 | 0.502E+00 | 1504 | 78 |
| 7995 | 0.218E+00 | 0.467E+00 | 1550 | 77 |
| 8159 | 0.206E+00 | 0.431E+00 | 1595 | 76 |
| 8260 | 0.199E+00 | 0.408E+00 | 1622 | 75 |
| 8398 | 0.190E+00 | 0.377E+00 | 1657 | 75 |
| 8474 | 0.180E+00 | 0.347E+00 | 1676 | 74 |
| 8600 | 0.168E+00 | 0.302E+00 | 1703 | 74 |
| 8688 | 0.160E+00 | 0.270E+00 | 1720 | 73 |
| 8827 | 0.149E+00 | 0.218E+00 | 1745 | 73 |
| 9129 | 0.127E+00 | 0.127E+00 | 1823 | 72 |
| 9356 | 0.108E+00 | 0.108E+00 | 1874 | 71 |
| 9734 | 0.920E-01 | 0.920E-01 | 1953 | 70 |
| 10409 | 0.578E-01 | 0.578E-01 | 2079 | 70 |
| 10484 | 0.639E-01 | 0.639E-01 | 2094 | 70 |
| 10514 | 0.525E+01 | 0.989E+01 | 2216 | 70 |
| 10559 | 0.796E+00 | 0.796E+00 | 2286 | 70 |
| 10574 | 0.0 | 0.0 | 721 | 70 |
| 10769 | 0.0 | 0.0 | 727 | 70 |
| 10784 | 0.206E+01 | 0.206E+01 | 2306 | 70 |
| 10814 | 0.436E+01 | 0.745E+01 | 2347 | 70 |
| 10874 | 0.480E+01 | 0.958E+01 | 2588 | 71 |
| 10904 | 0.107E+02 | 0.166E+02 | 2874 | 125 |
| 10915 | 0.176E+02 | 0.278E+02 | 306 | 119 |
| 10924 | 0.0 | 0.513E+01 | 308 | 113 |
| 10931 | 0.0 | 0.0 | 891 | 107 |
| 10962 | 0.0 | 0.0 | 891 | 83 |
| 10969 | 0.0 | 0.837E+02 | 315 | 79 |
| 10975 | 0.0 | 0.201E+03 | 312 | 75 |
| 10987 | 0.0 | 0.219E+03 | 304 | 72 |
| 11000 | 0.0 | 0.318E+02 | 304 | 72 |
| 11027 | 0.0 | 0.420E+02 | 305 | 72 |
| 11871 | 0.0 | 0.468E+02 | 303 | 70 |
| 13251 | 0.0 | 0.470E+02 | 303 | 71 |
| 13257 | 0.0 | 0.318E+03 | 309 | 70 |
| 13277 | 0.0 | 0.453E+02 | 303 | 71 |
| 15067 | 0.0 | 0.481E+02 | 303 | 70 |
| 15095 | 0.0 | 0.181E+01 | 302 | 70 |
| 15115 | 0.0 | 0.0 | 345 | 70 |
| 15410 | 0.0 | 0.0 | 345 | 70 |

Table A.2 Grand Gulf TC–MARCH2 output for input to TRAP-MELT

| Time (s) | Flows from core (g/s) | |
|---|---|---|
| | CsI | CsOH |
| 0 | 41.5 | 414 |
| 96 | 9.81 | 59.3 |
| 276 | 11.7 | 70.6 |
| 444 | 12.3 | 74.6 |
| 612 | 11.8 | 73.9 |
| 780 | 12.0 | 72.5 |
| 960 | 11.0 | 66.5 |
| 1150 | 10.4 | 62.7 |
| 1340 | 9.69 | 58.6 |
| 1550 | 8.57 | 51.8 |
| 1780 | 8.08 | 48.9 |
| 2070 | 7.10 | 43.0 |
| 2440 | 6.17 | 37.3 |
| 2810 | 5.70 | 34.5 |
| 3111 | 12.5 | 75.6 |
| 3290 | 15.9 | 96.0 |
| 3490 | 7.06 | 42.7 |
| 3760 | 0.98 | 5.93 |
| 4020 | 0.27 | 1.63 |
| 5350 | 0.08 | 0.5 |

Table A.3 Grand Gulf TC—MARCH2 output for input to TRAP-MELT

| Time (s) | Pressure (psia) | Average gas temperature (°F) | | | |
|---|---|---|---|---|---|
| | | Volume 1 | Volume 2 | Volume 3 | Volume 4 |
| 0 | 1370 | 640 | 597 | 590 | 582 |
| 135 | 1420 | 640 | 597 | 590 | 582 |
| 405 | 1520 | 640 | 597 | 590 | 582 |
| 675 | 1620 | 651 | 603 | 590 | 582 |
| 945 | 1720 | 651 | 603 | 590 | 582 |
| 1230 | 1830 | 651 | 603 | 590 | 582 |
| 1530 | 1930 | 661 | 608 | 590 | 582 |
| 1830 | 2030 | 661 | 608 | 590 | 582 |
| 2160 | 2120 | 661 | 608 | 590 | 582 |
| 2490 | 2210 | 669 | 612 | 590 | 582 |
| 2810 | 2300 | 679 | 615 | 583 | 585 |
| 3100 | 2960 | 1040 | 730 | 768 | 664 |
| 3360 | 1740 | 1830 | 1420 | 1420 | 1170 |
| 3630 | 568 | 1290 | 1420 | 1120 | 1240 |
| 3930 | 567 | 860 | 1080 | 836 | 1040 |
| 4250 | 567 | 686 | 812 | 697 | 832 |
| 4580 | 603 | 669 | 764 | 668 | 800 |
| 4890 | 613 | 675 | 755 | 667 | 805 |
| 5400 | 613 | 675 | 755 | 667 | 805 |

Table A.4 Grand Gulf TQUV—MERGE output from MARCH2

| Time* (s) | Flow rate from core (lb/s) | | Core exit temperature (°F) |
|---|---|---|---|
| | $H_2$ | Total | |
| 0 | 0.0441 | 11.6 | 1255 |
| 120 | 0.0661 | 9.95 | 1315 |
| 180 | 0.0799 | 9.26 | 1346 |
| 300 | 0.114 | 8.30 | 1411 |
| 360 | 0.136 | 7.79 | 1444 |
| 420 | 0.162 | 7.01 | 1476 |
| 480 | 0.156 | 131 | 1765 |
| 543 | 0.132 | 110 | 1848 |
| 605 | 0.118 | 93.8 | 1902 |
| 664 | 0.109 | 83.5 | 1945 |
| 725 | 0.104 | 76.1 | 1980 |
| 843 | 0.103 | 62.5 | 2047 |
| 901 | 0.0966 | 58.4 | 20731 |
| 1087 | 0.0750 | 44.7 | 2123 |
| 1200 | 0.0703 | 37.2 | 2148 |
| 1260 | 0.0701 | 34.4 | 2159 |
| 1382 | 0.0748 | 28.8 | 2190 |
| 1566 | 0.0957 | 22.9 | 2250 |
| 1622 | 0.109 | 21.5 | 2272 |
| 1809 | 0.225 | 16.0 | 2413 |
| 1874 | 0.285 | 15.0 | 2514 |
| 2222 | 0.756 | 7.73 | 2794 |
| 2281 | 0.812 | 6.70 | 2846 |
| 2642 | 0.863 | 3.30 | 3053 |
| 2704 | 0.0 | 0.0 | 0 |
| 3020 | 0.647 | 1.42 | 3064 |
| 3064 | 0.604 | 1.31 | 3072 |
| 3346 | 0.638 | 1.20 | 3150 |
| 3603 | 0.506 | 0.719 | 3197 |
| 3661 | 0.296 | 0.377 | 3202 |
| 3904 | 0.0802 | 0.0802 | 3219 |
| 3969 | 0.0 | 0.0 | 0 |
| 4287 | 0.0547 | 0.0547 | 3135 |
| 4335 | 0.0127 | 0.0127 | 3130 |
| 4550 | 0.0 | 7.5 | 3120 |
| 4910 | 0.0 | 24.7 | 3100 |
| 5280 | 0.0 | 67.8 | 2980 |
| 5650 | 0.0 | 79.0 | 2920 |

Table A.4 (Continued)

| Time* (s) | Flow rate from core (lb/s) | | Core exit temperature (°F) |
|---|---|---|---|
| | $H_2$ | Total | |
| 6010 | 0.0 | 47.3 | 2800 |
| 6350 | 0.0 | 10.3 | 2740 |
| 6720 | 0.0 | 3.0 | 2650 |
| 6843 | 0.0 | 1.4 | 2604 |
| 7090 | 0.0 | 0.95 | 500 |
| 7440 | 0.0 | 0.49 | 500 |

*Note: All entries after t = 4335 are from TRAP-MELT input, with $H_2$ = 0 assumed, and most temperatures assumed (exception is point at t = 6843).

Table A.5 Grand Gulf TQUV–MARCH2 output for input to TRAP-MELT

| Time (s) | Flows from core (g/s) | |
|---|---|---|
| | CsI | CsOH |
| 0 | 36.1 | 337 |
| 130 | 8.76 | 54.1 |
| 325 | 15.5 | 93.2 |
| 451 | 17.6 | 106 |
| 577 | 18.1 | 110 |
| 704 | 17.8 | 108 |
| 886 | 10.3 | 64.2 |
| 1090 | 11.6 | 70.4 |
| 1230 | 16.1 | 97.6 |
| 1380 | 12.5 | 75.6 |
| 1590 | 10.5 | 63.3 |
| 1860 | 8.08 | 48.9 |
| 2670 | 4.67 | 28.2 |
| 3040 | 7.07 | 42.8 |
| 3340 | 6.85 | 41.4 |
| 3630 | 1.33 | 8.0 |
| 3940 | 0.35 | 2.1 |
| 4300 | 0.18 | 1.1 |
| 6840 | 0.03 | 0.21 |

Table A.6 Grand Gulf TQUV–MARCH2 output for input to TRAP-MELT

| Time (s) | Pressure (psia) | Average gas temperature (°F) | | | |
|---|---|---|---|---|---|
| | | Volume 1 | Volume 2 | Volume 3 | Volume 4 |
| 0 | 100 | 2510 | 1690 | 1430 | 1050 |
| 204 | 81.9 | 2680 | 1730 | 1460 | 1050 |
| 619 | 56.4 | 2880 | 1800 | 1520 | 1040 |
| 1040 | 45.8 | 2970 | 1840 | 1550 | 914 |
| 1470 | 36.3 | 3150 | 1900 | 1580 | 1040 |
| 1890 | 32.4 | 3210 | 1940 | 1600 | 995 |
| 2300 | 31.0 | 3170 | 1948 | 1610 | 744 |
| 2690 | 78.2 | 3240 | 2090 | 1680 | 1300 |
| 3050 | 210 | 2670 | 2390 | 1920 | 1510 |
| 3420 | 327 | 422 | 2180 | 2150 | 1500 |
| 3790 | 345 | 431 | 1320 | 1740 | 1130 |
| 4150 | 261 | 407 | 936 | 1290 | 871 |
| 4490 | 84.6 | 321 | 931 | 1210 | 839 |
| 4860 | 39.0 | 268 | 935 | 1190 | 829 |
| 5230 | 31.0 | 253 | 937 | 1180 | 819 |
| 6300 | 26.0 | 240 | 938 | 1170 | 816 |
| 6900 | 25.0 | 240 | 938 | 1170 | 816 |

Table A.7 Peach Bottom AE–MERGE output for input to MARCH2

| Time (s) | Flow rate from core (lb/s) | | Core exit temperature (°F) |
|---|---|---|---|
| | $H_2$ | Total | |
| 0 | 0 | 0 | 1363 |
| 510 | 0.227 | 0.354 | 1363 |
| 690 | 0.219 | 0.337 | 1476 |
| 930 | 0.140 | 0.175 | 1568 |
| 1170 | 0.196 | 0.226 | 1746 |
| 1410 | 0.142 | 0.145 | 1865 |
| 1650 | 0.710 | 0.833 | 3141 |
| 1890 | 1.02 | 161 | 2610 |
| 2130 | 0.232 | 173 | 1178 |
| 2325 | 0.028 | 1.03 | 1606 |
| 2370 | 0 | 0 | 0 |
| 7000 | 0 | 0 | 0 |

Table A.8 Peach Bottom AE–MARCH2 output for input to TRAP-MELT

| Time (s) | Flows from core (g/s) | |
|---|---|---|
| | CsI | CsOH |
| 0 | 1.53 | 49.4 |
| 270 | 2.59 | 32.5 |
| 660 | 11.0 | 73.8 |
| 870 | 17.2 | 116 |
| 1050 | 18.5 | 124 |
| 1230 | 16.8 | 113 |
| 1410 | 14.8 | 99.6 |
| 1560 | 27.0 | 181 |
| 1680 | 28.9 | 194 |
| 1890 | 4.13 | 27.9 |
| 2340 | 1.92 | 12.9 |
| 3390 | 0.89 | 5.9 |
| 4500 | 1.56 | 10.5 |
| 5250 | 3.04 | 20.4 |
| 6300 | 1.47 | 9.9 |
| 6990 | 0.055 | 0.37 |

Table A.9 Peach Bottom AE–MARCH2 output for input to TRAP-MELT

| Time (s) | Pressure (psia) | Average gas temperature (°F) | | |
|---|---|---|---|---|
| | | Volume 1 | Volume 2 | Volume 3 |
| 0 | 38.2 | 930 | 265 | 265 |
| 60 | 34.6 | 930 | 707 | 366 |
| 180 | 31.8 | 930 | 504 | 471 |
| 300 | 30.9 | 930 | 496 | 376 |
| 420 | 30.5 | 1220 | 517 | 398 |
| 600 | 30.5 | 1445 | 544 | 432 |
| 780 | 30.5 | 1550 | 554 | 430 |
| 960 | 30.5 | 1645 | 560 | 425 |
| 1140 | 30.5 | 1750 | 567 | 442 |
| 1260 | 30.5 | 1820 | 582 | 451 |
| 1380 | 30.6 | 1900 | 613 | 475 |
| 1500 | 34.2 | 2290 | 1040 | 954 |
| 1620 | 68.5 | 3210 | 1990 | 1900 |
| 1740 | 104 | 3250 | 2330 | 2220 |
| 1880 | 122 | 2340 | 2200 | 2120 |
| 2030 | 44 | 1270 | 1580 | 1550 |
| 2180 | 25.2 | 957 | 1270 | 1250 |
| 2300 | 15.4 | 1240 | 1340 | 775 |
| 2360 | 15.4 | 1240 | 1340 | 775 |
| 7000 | 15.4 | 1240 | 1340 | 775 |

Table A.10 Peach Bottom TC2—MERGE output from MARCH2

| Time (s) | Flow rate from core (lb/s) | | Core exit temperature (°F) | Pressure (psia) |
|---|---|---|---|---|
| | Hydrogen | Total | | |
| 3514 | 0.0 | 0.0 | 690 | 1105 |
| 3736 | 0.0 | 0.0 | 690 | 1104 |
| 3742 | 0.180E+00 | 0.544E+00 | 1690 | 1104 |
| 3778 | 0.257E+00 | 0.841E+00 | 1815 | 1108 |
| 3814 | 0.524E+00 | 0.188E+01 | 1843 | 1111 |
| 3850 | 0.174E+01 | 0.665E+01 | 1939 | 1124 |
| 3871 | 0.482E+01 | 0.255E+02 | 2059 | 1118 |
| 3881 | 0.680E+01 | 0.396E+02 | 2225 | 1109 |
| 3896 | 0.411E+01 | 0.189E+02 | 2149 | 1079 |
| 3913 | 0.0 | 0.0 | 736 | 1099 |
| 4066 | 0.0 | 0.0 | 736 | 1098 |
| 4072 | 0.116E+00 | 0.211E+00 | 2089 | 1098 |
| 4108 | 0.395E+00 | 0.117E+01 | 2180 | 1100 |
| 4144 | 0.142E+01 | 0.515E+01 | 2276 | 1111 |
| 4162 | 0.637E+00 | 0.206E+01 | 2258 | 1116 |
| 4174 | 0.0 | 0.0 | 765 | 1116 |
| 4186 | 0.277E+00 | 0.642E+00 | 2136 | 1117 |
| 4222 | 0.347E+00 | 0.854E+00 | 2257 | 1121 |
| 4258 | 0.391E+00 | 0.957E+00 | 2270 | 1125 |
| 4294 | 0.826E+00 | 0.250E+01 | 2294 | 1131 |
| 4301 | 0.414E+01 | 0.153E+02 | 2416 | 1099 |
| 4313 | 0.932E+01 | 0.167E+03 | 2940 | 1120 |
| 4328 | 0.916E+01 | 0.418E+02 | 2998 | 1101 |
| 4351 | 0.378E+01 | 0.141E+02 | 3031 | 1111 |
| 4356 | 0.0 | 0.0 | 883 | 1111 |
| 4523 | 0.0 | 0.0 | 883 | 1110 |
| 4529 | 0.418E+00 | 0.877E+00 | 2859 | 1110 |
| 4565 | 0.146E+01 | 0.406E+01 | 3061 | 1121 |
| 4601 | 0.120E+01 | 0.266E+01 | 3104 | 1132 |
| 4612 | 0.414E+01 | 0.134E+02 | 3146 | 1110 |
| 4622 | 0.826E+01 | 0.127E+03 | 3720 | 1120 |
| 4638 | 0.835E+01 | 0.375E+02 | 3748 | 1090 |
| 4657 | 0.475E+01 | 0.149E+02 | 3910 | 1123 |
| 4661 | 0.0 | 0.0 | 1063 | 1123 |
| 4701 | 0.0 | 0.0 | 1063 | 1120 |
| 4707 | 0.617E+00 | 0.132E+01 | 3651 | 1121 |
| 4743 | 0.174E+01 | 0.385E+01 | 3812 | 1138 |
| 4748 | 0.728E+01 | 0.231E+02 | 3800 | 1112 |
| 4759 | 0.716E+01 | 0.397E+02 | 3955 | 1122 |
| 4778 | 0.754E+01 | 0.391E+02 | 4079 | 1090 |

Table A.10 (Continued)

| Time (s) | Flow rate from core (lb/s) | | Core exit temperature (°F) | Pressure (psia) |
|---|---|---|---|---|
| | Hydrogen | Total | | |
| 4790 | 0.500E+01 | 0.124E+02 | 4120 | 1129 |
| 4794 | 0.0 | 0.0 | 1238 | 1129 |
| 4821 | 0.0 | 0.0 | 1238 | 1127 |
| 4827 | 0.564E+00 | 0.118E+01 | 3865 | 1128 |
| 4863 | 0.213E+01 | 0.470E+01 | 3983 | 1146 |
| 4869 | 0.787E+01 | 0.441E+02 | 3998 | 1124 |
| 4878 | 0.670E+01 | 0.328E+02 | 4053 | 1139 |
| 4890 | 0.0 | 0.0 | 2101 | 1119 |
| 4905 | 0.713E+01 | 0.124E+03 | 4004 | 1132 |
| 5028 | 0.131E+01 | 0.282E+01 | 3967 | 1150 |
| 5033 | 0.567E+01 | 0.171E+02 | 3970 | 1122 |
| 5041 | 0.645E+01 | 0.920E+02 | 4016 | 1141 |
| 5055 | 0.738E+01 | 0.608E+02 | 4014 | 1106 |
| 5071 | 0.408E+01 | 0.112E+02 | 4040 | 1135 |
| 5075 | 0.0 | 0.0 | 1644 | 1135 |
| 5106 | 0.0 | 0.0 | 1644 | 1133 |
| 5112 | 0.870E+00 | 0.184E+01 | 3868 | 1135 |
| 5142 | 0.150E+01 | 0.324E+01 | 3989 | 1150 |
| 5148 | 0.662E+01 | 0.232E+02 | 3985 | 1122 |
| 5156 | 0.650E+01 | 0.786E+02 | 4025 | 1150 |
| 5169 | 0.673E+01 | 0.300E+02 | 4028 | 1116 |
| 5186 | 0.776E+01 | 0.231E+02 | 3153 | 1135 |
| 5193 | 0.256E+02 | 0.548E+02 | 559 | 1166 |
| 5195 | 0.0 | 0.219E+02 | 560 | 1149 |
| 5209 | 0.0 | 0.303E+03 | 558 | 1122 |
| 5246 | 0.0 | 0.124E+03 | 563 | 1161 |
| 5673 | 0.0 | 0.466E+02 | 562 | 1154 |
| 5709 | 0.0 | 0.145E+03 | 563 | 1156 |
| 6904 | 0.0 | 0.246E+02 | 561 | 1138 |
| 7589 | 0.0 | 0.117E+02 | 564 | 1168 |

Table A.11 Peach Bottom TC2—MARCH2 output for input to TRAP-MELT

| Time (s) | Flows from core (g/s) | |
|---|---|---|
| | CsI | CsOH |
| 3500 | 0 | 0 |
| 3504 | 72.5 | 667.1 |
| 3548 | 24.6 | 163.4 |
| 3676 | 13.0 | 87.0 |
| 3833 | 15.0 | 100.7 |
| 3968 | 17.3 | 116.3 |
| 4132 | 10.7 | 72.3 |
| 4295 | 18.0 | 122.7 |
| 4425 | 15.9 | 108.5 |
| 4585 | 11.9 | 83.4 |
| 4735 | 18.0 | 126.4 |
| 4859 | 16.5 | 113.0 |
| 5027 | 10.3 | 70.9 |
| 5173 | 22.8 | 171.6 |
| 5248 | 31.2 | 227.7 |
| 5361 | 2.7 | 19.6 |
| 6516 | 0.11 | 0.83 |
| 7587 | 0.007 | 0.05 |

Table A.12 Peach Bottom TC2—MARCH2 output for input to TRAP-MELT

| Time (s) | Pressure (psia) | Average gas temperature (°F) | | | |
|---|---|---|---|---|---|
| | | Volume 1 | Volume 2 | Volume 3 | Volume 4 |
| 3500 | 1290 | 1090 | 884 | 740 | 671 |
| 3700 | 1290 | 1090 | 884 | 740 | 671 |
| 3706 | 1290 | 1090 | 884 | 740 | 671 |
| 3913 | 1490 | 1190 | 921 | 779 | 697 |
| 4114 | 1470 | 1190 | 895 | 790 | 672 |
| 4315 | 1710 | 1540 | 1300 | 913 | 816 |
| 4523 | 1940 | 1600 | 1200 | 936 | 793 |
| 4725 | 2380 | 1830 | 1250 | 1020 | 802 |
| 4923 | 2490 | 2140 | 1470 | 1240 | 955 |
| 5130 | 2480 | 2210 | 1640 | 1340 | 978 |
| 5329 | 567 | 968 | 1260 | 1420 | 1290 |
| 5535 | 567 | 764 | 1060 | 1250 | 1200 |
| 5738 | 567 | 651 | 859 | 1040 | 1100 |
| 5938 | 567 | 607 | 741 | 887 | 986 |
| 6547 | 568 | 576 | 601 | 649 | 718 |
| 7360 | 569 | 591 | 607 | 615 | 703 |
| 7600 | 569 | 591 | 607 | 615 | 703 |

Table A.13 Sequoyah TB—MERGE output from MARCH2

| Time (s) | Flow rate from core (lb/s) | | Core exit temperature (°F) |
|---|---|---|---|
| | $H_2$ | Total | |
| 19356 | 0.112 | 12.6 | 2460 |
| 19656 | 0.607 | 4.44 | 2637 |
| 19956 | 0.627 | 2.23 | 3010 |
| 20256 | 0.730 | 0.812 | 3352 |
| 20556 | 0.687 | 0.728 | 3505 |
| 20856 | 0.825 | 0.900 | 3617 |
| 21162 | 1.525 | 2.02 | 3772 |
| 21366 | 0 | 75.85 | 3288 |
| 21426 | 0 | 115.2 | 3210 |
| 21498 | 0 | 123.7 | 3135 |
| 21558 | 0 | 124.7 | 3070 |
| 21636 | 0 | 142.6 | 2991 |
| 21720 | 0 | 128.3 | 2904 |
| 21804 | 0 | 128.3 | 2813 |
| 21894 | 0 | 126.8 | 2728 |
| 21954 | 0 | 130.85 | 2667 |
| 22014 | 0 | 131.75 | 2602 |
| 22086 | 0 | 111.7 | 2528 |
| 22176 | 0 | 106.1 | 2440 |
| 22260 | 0 | 118.4 | 2355 |
| 22338 | 0 | 117.6 | 2280 |
| 22416 | 0 | 100.65 | 2203 |

Table A.14 Sequoyah TB—MARCH2 output for input to TRAP-MELT

| Time (s) | Flows from core (g/s) | |
|---|---|---|
| | CsI | CsOH |
| 19400 | 0 | 0 |
| 19643 | 16.39 | 146.2 |
| 19748 | 10.00 | 64.3 |
| 19913 | 17.00 | 103.8 |
| 20033 | 20.0 | 114.9 |
| 20145 | 20.9 | 121.9 |
| 20250 | 22.0 | 128.0 |
| 20355 | 22.5 | 132.3 |
| 20460 | 21.6 | 127.3 |
| 20565 | 20.3 | 119.6 |
| 20685 | 16.5 | 98.2 |
| 20828 | 15.0 | 88.9 |
| 20985 | 12.9 | 78.1 |
| 21163 | 10.4 | 63.8 |
| 21307 | 20.4 | 133.1 |
| 21481 | 0.67 | 4.3 |
| 22012 | 0.045 | 0.28 |
| 22414 | 0.002 | 0.01 |

Table A.15 Sequoyah TB—MARCH2 output for input to TRAP-MELT

| Time (s) | Pressure (psia) | Average gas temperature (°F) | | | |
|---|---|---|---|---|---|
| | | Volume 1 | Volume 2 | Volume 3 | Volume 4 |
| 19400 | 1223 | 1830 | 1100 | 1050 | 671 |
| 19782 | 1223 | 1830 | 1100 | 1050 | 671 |
| 19923 | 1254 | 1910 | 1120 | 1070 | 675 |
| 20063 | 1282 | 1990 | 1150 | 1090 | 680 |
| 20198 | 1305 | 2090 | 1170 | 1110 | 676 |
| 20337 | 1327 | 2150 | 1210 | 1140 | 679 |
| 20475 | 1345 | 2180 | 1240 | 1170 | 681 |
| 20614 | 1360 | 2220 | 1280 | 1200 | 685 |
| 20753 | 1370 | 2240 | 1310 | 1240 | 690 |
| 20891 | 1407 | 2280 | 1370 | 1310 | 694 |
| 21030 | 1485 | 2310 | 1430 | 1370 | 706 |
| 21167 | 1588 | 2360 | 1500 | 1440 | 714 |
| 21306 | 1911 | 605 | 1010 | 1040 | 730 |
| 21444 | 2102 | 613 | 758 | 779 | 727 |
| 21584 | 2043 | 611 | 667 | 680 | 721 |
| 22419 | 1999 | 608 | 619 | 620 | 664 |

Table A.16 Surry TMLB'—MERGE output from MARCH2

| Time (s) | Flow rate from core (lb/s) Hydrogen | Total | Core exit temperature (°F) | Pressure (psia) |
|---|---|---|---|---|
| 0 | 0.000E+00 | 0.298E+04 | 580 | 2250 |
| 2640 | 0.000E+00 | 0.667E+02 | 564 | 1599 |
| 2670 | 0.000E+00 | 0.369E+02 | 564 | 1619 |
| 2820 | 0.000E+00 | 0.802E+01 | 573 | 1816 |
| 5835 | 0.000E+00 | 0.784E+02 | 660 | 2369 |
| 5850 | 0.668E-07 | 0.782E+02 | 660 | 2369 |
| 5955 | 0.567E-06 | 0.691E+02 | 669 | 2369 |
| 6060 | 0.246E-05 | 0.518E+02 | 703 | 2369 |
| 6135 | 0.779E-05 | 0.409E+02 | 746 | 2369 |
| 6195 | 0.236E-04 | 0.335E+02 | 766 | 2369 |
| 6270 | 0.963E-04 | 0.266E+02 | 836 | 2369 |
| 6330 | 0.288E-03 | 0.224E+02 | 889 | 2369 |
| 6345 | 0.378E-03 | 0.216E+02 | 900 | 2369 |
| 6390 | 0.840E-03 | 0.191E+02 | 935 | 2369 |
| 6405 | 0.109E-02 | 0.184E+02 | 945 | 2369 |
| 6495 | 0.436E-02 | 0.149E+02 | 1009 | 2368 |
| 6570 | 0.105E-01 | 0.129E+02 | 1063 | 2368 |
| 6645 | 0.207E-01 | 0.110E+02 | 1116 | 2368 |
| 6705 | 0.327E-01 | 0.997E+01 | 1162 | 2368 |
| 6810 | 0.668E-01 | 0.786E+01 | 1241 | 2367 |
| 6900 | 0.121E+00 | 0.665E+01 | 1315 | 2367 |
| 6975 | 0.205E+00 | 0.543E+01 | 1380 | 2367 |
| 7020 | 0.302E+00 | 0.420E+01 | 1413 | 2366 |
| 7050 | 0.461E+00 | 0.252E+01 | 1426 | 2366 |
| 7185 | 0.434E+00 | 0.140E+01 | 1527 | 2366 |
| 7335 | 0.330E+00 | 0.526E+00 | 1638 | 2366 |
| 7545 | 0.202E+00 | 0.202E+00 | 1745 | 2365 |
| 7965 | 0.876E-01 | 0.876E-01 | 1892 | 2364 |
| 8235 | 0.000E+00 | 0.000E+00 | 663 | 2363 |
| 8340 | 0.000E+00 | 0.000E+00 | 663 | 2343 |
| 8400 | 0.799E+00 | 0.829E+00 | 2059 | 2354 |
| 8595 | 0.159E+01 | 0.202E+01 | 2689 | 2363 |
| 8625 | 0.508E+01 | 0.206E+02 | 3413 | 2363 |
| 8685 | 0.387E+01 | 0.705E+02 | 3852 | 2366 |
| 8700 | 0.675E+00 | 0.106E+03 | 660 | 2366 |
| 8715 | 0.000E+00 | 0.107E+03 | 660 | 2367 |
| 9045 | 0.000E+00 | 0.000E+00 | 944 | 2370 |

Table A.17 Surry TMLB′—MARCH2 output for input to TRAP-MELT

| Time (s) | Flows from core (g/s) | |
|---|---|---|
| | CsI | CsOH |
| 0 | 40.5 | 368 |
| 60 | 25.8 | 130 |
| 150 | 32.3 | 163 |
| 240 | 26.2 | 132 |
| 360 | 20.8 | 105 |
| 480 | 16.1 | 80.9 |
| 630 | 13.3 | 66.8 |
| 810 | 11.4 | 57.3 |
| 1020 | 8.1 | 41.0 |
| 1320 | 6.1 | 30.6 |
| 1650 | 7.2 | 36.1 |
| 2070 | 1.7 | 8.3 |
| 2340 | 0.7 | 3.7 |

Table A.18 Surry TMLB′—MARCH2 output for input to TRAP-MELT

| Time (s) | Pressure (psia) | Average gas temperature (°F) | |
|---|---|---|---|
| | | Volume 1 | Volume 2 |
| 0 | 2370 | 1470 | 862 |
| 45 | 2365 | 1500 | 866 |
| 143 | 2360 | 1560 | 873 |
| 248 | 2358 | 1640 | 878 |
| 368 | 2356 | 1690 | 881 |
| 488 | 2354 | 1740 | 883 |
| 645 | 2353 | 1800 | 888 |
| 833 | 2352 | 1850 | 891 |
| 1020 | 2351 | 900 | 891 |
| 1240 | 2350 | 788 | 887 |
| 1470 | 2340 | 1780 | 930 |
| 1570 | 2360 | 2240 | 1090 |
| 1680 | 2365 | 3090 | 1730 |
| 1770 | 2370 | 1230 | 1200 |
| 1900 | 2370 | 660 | 758 |
| 1980 | 2370 | 660 | 719 |
| 2010 | 2370 | 660 | 756 |
| 2340 | 2370 | 660 | 784 |

Table A.19 Surry AB—MARCH2 output for input to TRAP-MELT

| Time (s) | Flow rate from core (lb/s) | | Core exit temperature (°F) |
|---|---|---|---|
| | $H_2$ | Total | |
| 0 | 0 | 0 | 1228 |
| 246 | 0.392 | 0.392 | 1228 |
| 312 | 0.353 | 0.353 | 1280 |
| 576 | 0.270 | 0.270 | 1471 |
| 906 | 0.233 | 0.233 | 1701 |
| 1170 | 0 | 40.3 | 3688 |
| 1230 | 1.393 | 40.7 | 3661 |
| 1470 | 6.083 | 40.25 | 3571 |
| 2070 | 0 | 40.7 | 3731 |
| 2706 | 0 | 0 | 3500 |
| 5000 | 0 | 0 | 3500 |

Table A.20 Surry AB—MARCH2 output for input to TRAP-MELT

| Time (s) | Flows from core (g/s) | |
|---|---|---|
| | CsI | CsOH |
| 0 | 162 | 1100 |
| 36 | 35.1 | 178 |
| 96 | 37.6 | 190 |
| 156 | 34.0 | 172 |
| 228 | 29.0 | 146 |
| 300 | 26.7 | 135 |
| 384 | 22.9 | 115 |
| 480 | 19.7 | 99.3 |
| 588 | 16.5 | 83.3 |
| 720 | 13.3 | 66.9 |
| 900 | 8.68 | 43.8 |
| 1180 | 4.4 | 22.3 |
| 1450 | 1.1 | 5.3 |
| 1630 | 0.62 | 3.2 |
| 1880 | 0.35 | 1.8 |
| 2520 | 0.21 | 1.1 |
| 4030 | 0.04 | 0.22 |
| 5190 | 0 | 0 |

Table A.21 Surry AB—MARCH2 output for input to TRAP-MELT

| Time (s) | Pressure (psia) | Average gas Temperature (°F) | |
|---|---|---|---|
| | | Volume 1 | Volume 2 |
| 0 | 35.6 | 1040 | 724 |
| 198 | 34.6 | 0 | 803 |
| 330 | 34.0 | 1300 | 863 |
| 462 | 34.0 | 1400 | 920 |
| 726 | 32.5 | 1580 | 1010 |
| 858 | 32.1 | 1670 | 1060 |
| 990 | 31.9 | 1920 | 1200 |
| 1120 | 33.6 | 1010 | 974 |
| 1250 | 34.5 | 258 | 517 |
| 1390 | 35.5 | 260 | 419 |
| 1520 | 36.8 | 262 | 374 |
| 1650 | 37.6 | 263 | 352 |
| 2040 | 39.6 | 266 | 327 |
| 2280 | 40.9 | 267 | 321 |
| 2340 | 41.1 | 257 | 323 |
| 5120 | 41.1 | 257 | 323 |

Table A.22 Grand Gulf—Compartment volumes for sequences TC and TQUV

| Control volume | Volume ($ft^3$) | |
|---|---|---|
| | TC | TQUV |
| Core | 1728 | 1728 |
| Steam separators | 3357 | 3357 |
| Steam dryers | 3335 | 3335 |
| Upper annulus | 2030 | 2030 |
| Relief line | 208 | 208 |

Table A.23 Peach Bottom—Compartment volumes for sequences TC and AE

| TC | | AE | |
|---|---|---|---|
| Control volume | Volume ($ft^3$) | Control volume | Volume ($ft^3$) |
| Core | 1360 | Core | 1728 |
| Shroud head | 1170 | Steam separator | 580 |
| Pipes and separators | 582 | Upper outer annulus | 2030 |
| Steam dryers | 3000 | | |
| Upper outer annulus | 1000 | | |
| Lower outer annulus | 1000 | | |
| Steam lines | 1080 | | |
| Relief lines | 622 | | |

Table A.24 Sequoyah—Compartment volumes for sequence TBA

| Control volume | Volume ($ft^3$) |
|---|---|
| Core | 1020 |
| Grid plate | 70.01 |
| Guide tubes | 85.70 |
| Upper support plate | 511 |
| Core barrel | 857 |

Table A.25 Surry—Compartment volumes for sequences AB and TMLB

| AB | | TMLB | |
|---|---|---|---|
| Control volume No. | Volume ($ft^3$) | Control volume No. | Volume ($ft^3$) |
| 1 | 589 | 1 | 589 |
| 2 | 100 | 2 | 100 |
| 3 | 506 | 3 | 506 |
| 4 | 79 | 4 | 230 |
| 5 | 150 | 6 | 1301 |

# Appendix B. Kinetic and Equilibrium Calculations

## B.1 Kinetics of Cs-I-$H_2$-$H_2O$ Reactions

Twenty reactions (ten reversible equations) were chosen to represent the kinetic behavior of cesium and iodine species. In a more comprehensive study of the rates of formation of CsOH and CsI under accident conditions, Wren used 152 reactions.[30] In that study, he concluded that in a CANDU reactor primary heat transport system under accident conditions, CsI and CsOH would form in $<10^{-2}$ s. In the present study, the kinetic calculations are used only as a guide in determining which control volumes reached equilibrium (i.e., those control volumes in which the residence times of cesium and iodine species were sufficiently long that the species concentrations did not vary with time).

The data on equilibrium thermodynamics are generally more reliable than data on rate constants. For this reason, equilibrium thermochemical calculations were performed in addition to the rate calculations.

The rate constants for the 20 reactions given in Table B.1 is the Arrhenius form

$$K = A \exp\left(-\frac{E_{act}}{RT}\right) \qquad \text{(B.1)}$$

where

$K$ = rate constant,
$A$ = preexponential or frequency factor,
$E_{act}$ = activation energy.

The rate constant equation written in this way assumes that there is little or no temperature dependence of $A$ or $E_{act}$ over the temperature range of interest.

In reactions of the type C + D ⇌ E + F, the rate constants for the forward and reverse reactions can satisfy the requirements of the equilibrium constant. The requirements of the equilibrium constraint to maintain $A$ and $E_{act}$ independent of temperature can be obtained as described in the following manipulation. The standard free energy change can often be fitted over a temperature interval by the simple linear relation

$$\Delta G^{o}_{F_{rxn}} = a + bT \qquad \text{(B.2)}$$

where

$\Delta G^{o}_{F_{rxn}}$ = standard free energy change of reaction,
$a, b$ = constants fit over the same temperature interval.

If we adopt this means of expressing $\Delta G^{o}_{F_{rxn}}$, then

$$\Delta G^{o}_{F_{rxn}} = a + bT = RT \ln K_{eq} = -RT \ln \frac{K_F}{K_R} \qquad \text{(B.3)}$$

where

$K_{eq}$ = equilibrium constant,
$K_F, K_R$ = rate constant for the forward and reverse reactions.

Equation B.3 can be rearranged as

$$K_F = \exp\left[-\left(\frac{a}{RT} + \frac{b}{R}\right)\right] \cdot K_R \qquad \text{(B.4)}$$

The rate constants for the forward and reverse reactions are expressed as

$$K_F = A \exp\left(-\frac{E_{act_F}}{RT}\right) \qquad \text{(B.5)}$$

$$K_R = A' \exp\left(-\frac{E_{act_R}}{RT}\right) \qquad \text{(B.6)}$$

Inserting Equations B.5 and B.6 into B.4 gives

$$A \exp\left(-\frac{E_{act_F}}{RT}\right) = \exp\left[-\left(\frac{a}{RT} + \frac{b}{R}\right)\right] \cdot A' \exp\left(-\frac{E_{act_R}}{RT}\right) \qquad \text{(B.7)}$$

or

**Table B.1 Reaction rate constants**

| Reaction | Rate constant* at 1000 K (1341°F) | Frequency factor | References |
|---|---|---|---|
| 1. $CsI + H_2O \rightarrow CsOH + HI$ | $2.12 \times 10^{-23}$ | $1.57 \times 10^{-12}$ | |
| 2. $CsOH + HI \rightarrow CsI + H_2O$ | $1.00 \times 10^{-15}$ | 1.00 × 10-11 | 32 |
| 3. $2HI \rightarrow I_2 + H_2$ | $2.42 \times 10^{-20}$ | $1.00 \times 10^{-10}$ | 33 |
| 4. $I_2 + H_2 \rightarrow 2HI$ | $3.01 \times 10^{-19}$ | $1.66 \times 10^{-10}$ | 33 |
| 5. $I + I + M \rightarrow I_2 + M$ | $1.15 \times 10^{-33}$ | $3.17 \times 10^{-34}$ | |
| 6. $M + I_2 \rightarrow I + I + M$ | $2.56 \times 10^{-17}$ | $3.14 \times 10^{-10}$ | |
| 7. $I + H_2 \rightarrow HI + H$ | $2.19 \times 10^{-17}$ | $2.64 \times 10^{-10}$ | |
| 8. $HI + H \rightarrow I + H_2$ | $5.54 \times 10^{-11}$ | $7.4 \times 10^{-11}$ | |
| 9. $HI + I \rightarrow H + I_2$ | $4.66 \times 10^{-18}$ | $3.59 \times 10^{-10}$ | 34 |
| 10. $H + I_2 \rightarrow HI + I$ | $6.0 \times 10^{-10}$ | $6.0 \times 10^{-10}$ | 34, 35 |
| 11. $H + H + M \rightarrow H_2 + M$ | $1.25 \times 10^{-35}$ | $2.31 \times 10^{-33}$ | |
| 12. $M + H_2 \rightarrow H + H + M$ | $1.9 \times 10^{-29}$ | $4.98 \times 10^{-9}$ | |
| 13. $Cs + I + M \rightarrow CsI + M$ | $3.7 \times 10^{-33}$ | $6.44 \times 10^{-31}$ | |
| 14. $M + CsI \rightarrow Cs + I + M$ | $1.6 \times 10^{-22}$ | $5.37 \times 10^{-9}$ | |
| 15. $Cs + HI \rightarrow CsI + H$ | $2.00 \times 10^{-11}$ | $2.00 \times 10^{-11}$ | 32, 35 |
| 16. $CsI + H \rightarrow Cs + HI$ | $2.53 \times 10^{-13}$ | $2.82 \times 10^{-13}$ | |
| 17. $Cs + H_2O \rightarrow CsOH + H$ | $1.70 \times 10^{-16}$ | $1.11 \times 10^{-9}$ | |
| 18. $CsOH + H \rightarrow Cs + H_2O$ | $1.00 \times 10^{-10}$ | $1.00 \times 10^{-10}$ | 32 |
| 19. $Cs + I_2 \rightarrow CsI + I$ | $8.81 \times 10^{-10}$ | $8.81 \times 10^{-10}$ | 32 |
| 20. $CsI + I \rightarrow Cs + I_2$ | $8.66 \times 10^{-20}$ | $7.43 \times 10^{-12}$ | |

*Units are $s^{-1}$, $cm^3 \cdot molecule^{-1}\ s^{-1}$, and $cm^6 \cdot molecule^{-2}\ s^{-1}$ for first-, second-, and third-order reactions, respectively. M, the collision molecule, is the total of the $H_2$ and $H_2O$ molecular concentrations (molecules/$cm^3$).

$$\ln A - \frac{E_{act_F}}{RT} = \ln A' - \left(\frac{a}{RT} + \frac{b}{R}\right) - \frac{E_{act_R}}{RT} \qquad \text{(B.8)}$$

then

$$\ln A - \ln A' = \frac{E_{act_F} - E_{act_R}}{RT} - \left(\frac{a}{RT} + \frac{b}{R}\right) \qquad \text{(B.9)}$$

Assuming that $\ln A - \ln A' = -b/R$, then Equation B.9 becomes

$$\ln A - \ln A' = -\frac{b}{R} = \frac{E_{act_F} - E_{act_R}}{RT} - \left(\frac{a}{RT} + \frac{b}{R}\right) \qquad \text{(B.10)}$$

which yields

$$E_{act_F} - E_{act_R} = a \qquad \text{(B.11)}$$

Thus, fitting the standard free energy change of reaction to a linear form with temperature and assuming the difference in the natural log of the frequency factor for the forward and reverse reactions is equal to $-b/R$, then rate constants can be expressed in the Arrhenius form and satisfy the equilibrium constraint. Standard free energies of reaction in the form of $\Delta G^o = a + bT$ are given in Table B.2. These data were obtained from the FACT system.[3] The FACSIMILE computer program was used to perform the rate calculations.

## B.2 Equilibrium Calculations in the Cs-I-$H_2$-$H_2O$ System

The species considered in the equilibrium calculations include (gases) $H_2$, $H_2O$, CsOH, CsI, Cs, H, HI, I, and $I_2$; and (liquids) CsI, CsOH, Cs, and $I_2$. The calculations were performed with the EQUILIB routine of the FACT system. This method of calculation was chosen because it is readily accessible to anyone in North America and because the thermochemical data base of FACT comes from standard assessed sources such as JANAF[36] and Barin and Knacke.[37] Thermochemical data for CsOH are not part of the FACT[3] data base, and values from JANAF were inserted into a user's data base for these calculations.

The 13 species used in the equilibrium calculations are the same as those used in the kinetic calculations. Iodine ratios such as HI/CsI are very similar in the equilibrium calculations and in the kinetic calculations, primarily because the bimolecular rate constants are consistent with the equilibrium constants.

**Table B.2 Standard free energy of reaction 500 to 1200 K (441 to 1701°F) written as $\Delta G^o_{F_{rxn}} = a + bT$, exothermic reaction expressed left to right (Energy in joules)**

| Reaction | *a* | *b* |
|---|---|---|
| $CsOH + HI \rightleftharpoons CsI + H_2O$ | $-1.31368 \times 10^5$ | $-1.54100 \times 10^1$ |
| $I_2 + H_2 \rightleftharpoons 2HI$ | $-1.30038 \times 10^4$ | $-1.48455 \times 10^1$ |
| $HI + H \rightleftharpoons I + H_2$ | $-1.37991 \times 10^5$ | $+1.05761 \times 10^1$ |
| $H + I_2 \rightleftharpoons HI + I$ | $-1.50995 \times 10^5$ | $-4.26918 \times 10^0$ |
| $Cs + HI \rightleftharpoons CsI + H$ | $-8.80264 \times 10^2$ | $-3.54386 \times 10^1$ |
| $CsOH + H \rightleftharpoons Cs + H_2O$ | $-1.30488 \times 10^5$ | $+2.00288 \times 10^1$ |
| $Cs + I_2 \rightleftharpoons CsI + I$ | $-1.51875 \times 10^5$ | $-3.97080 \times 10^1$ |

# Appendix C. Fitting of Radiolysis Data

Data from Lin[14] are listed in Table C.1 and shown in Figure C.1. The fraction of $I^-$ converted by radiolysis to $I_2$ must satisfy

$$\lim_{pH \to \infty} F = 0 \qquad \lim_{pH \to -\infty} F = 1 \qquad \text{(C.1a,b)}$$

which are identical to the conditions

$$\lim_{pH \to \infty} \ln\left(\frac{1}{F} - 1\right) = \infty \qquad \lim_{pH \to -\infty} \ln\left(\frac{1}{F} - 1\right) = -\infty$$

As shown in Figure C.1, there is a highly linear relationship between $\ln(\frac{1}{F} - 1)$ and pH. Using the data in Table C.1, a linear least-squares fit of the form

$$\ln\left(\frac{1}{F} - 1\right) = \alpha \cdot pH + \beta$$

yielded the values $\alpha = 1.72$ and $\beta = -6.08$ with a correlation coefficient of 0.94.

**Table C.1 Radiolysis data* for formation of $I_2$**

| Initial concentration (mol/L) | Initial pH | Conversion (%) |
|---|---|---|
| $10^{-3}$ | 2 | 88.2 |
| | 3 | 81.8 |
| | 4 | 8.6 |
| | 5 | 2.4 |
| | 6 | 2.4 |
| $10^{-4}$ | 3 | 93.8 |
| | 5 | 8.0 |
| | 6.6 | 1.7 |
| $10^{-5}$ | 2 | 89.1 |
| | 3 | 77.9 |
| | 4 | 44.4 |
| | 5 | 6.9 |
| | 6.3 | 0.3 |

*Taken from C. C. Lin.[14]

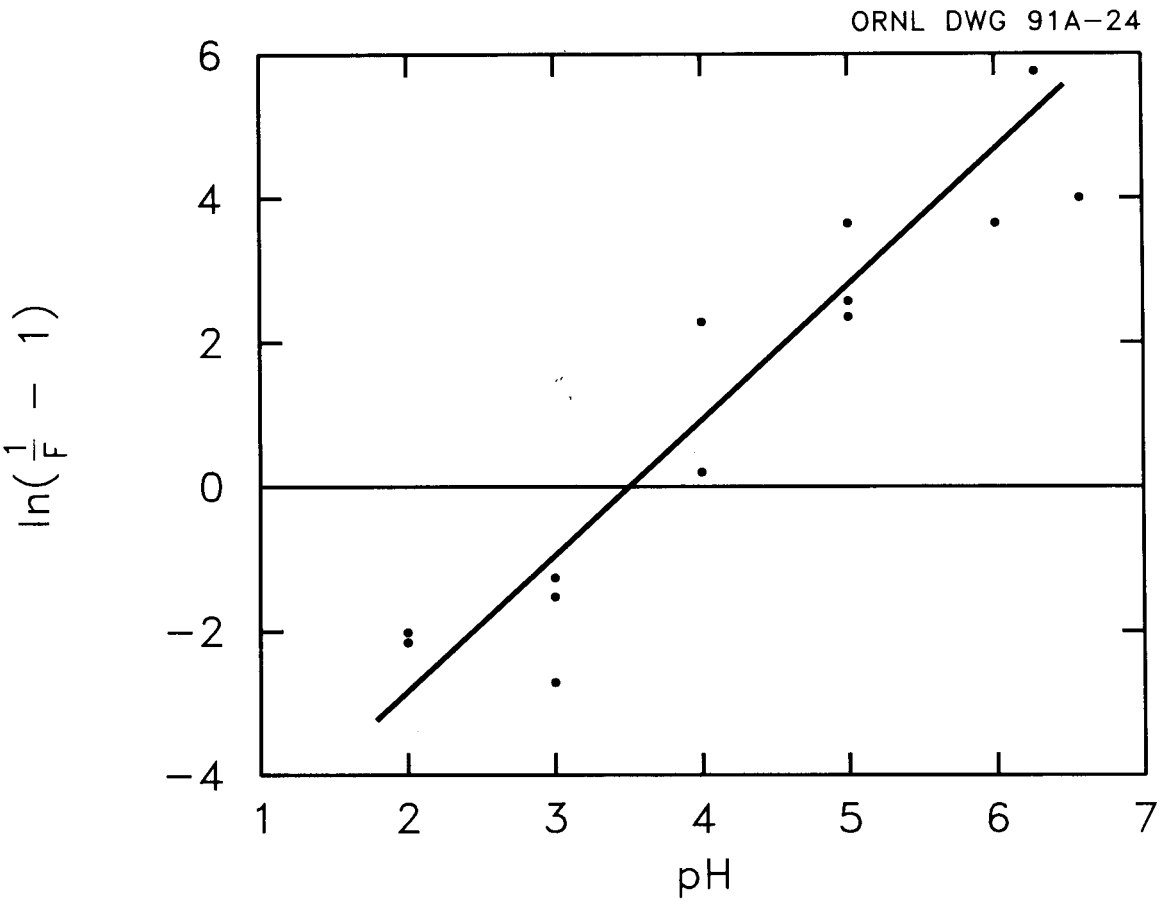


Figure C.1. Data fitting for radiolytic conversion of $I^-$ to $I_2$ (data from U.S. Nuclear Regulatory Commission, Regulation Guide 1.4, "Assumptions Used for Evaluating the Potential Radiological Consequences of a Loss-of-Coolant Accident for Pressurized Water Reactors")

# Appendix D. Fission Product Release Tables

Table D.1. Fission product inventories for selected plants*

| Nuclide group | | Total core inventory (kg) | | | |
|---|---|---|---|---|---|
| | | Grand Gulf | Peach Bottom | Sequoyah | Surry |
| 1 | I | 17.7 | 16.6 | 15.2 | 12.4 |
| 2 | Cs | 244.8 | 230.3 | 184.7 | 145.7 |
| 3 | Te | 37.1 | 34.9 | 31.7 | 25.4 |
| 4 | Sr | 66.7 | 62.7 | 60.9 | 47.6 |
| 5 | Ba | 112 | 105 | 77.7 | 61.2 |
| 6 | Ru | 621 | 584 | 470 | 369 |
| 7 | Ce | 221 | 208 | 167 | 131 |
| 8 | La | 1724 | 2404 | 1313 | 855 |
| 9 | Xe | 439 | 413 | 347 | 273 |

*Taken from References 1 and 2.

Table D.2. Bounding values for fractions of core inventory released into containment*

| Fission product group | PWR releases into containment | | | | BWR releases into containment | | | |
|---|---|---|---|---|---|---|---|---|
| | From primary system** | | From core-concrete interaction | | From primary system** | | From core-concrete interaction | |
| | High RCS pressure | Low RCS pressure | Limestone concrete | Basaltic concrete | High RCS pressure | Low RCS pressure | Limestone concrete | Basaltic concrete |
| I | 0.45 | 0.77 | 0.15 | 0.15 | 0.70 | 0.77 | 0.15 | 0.15 |
| Cs | 0.42 | 0.77 | 0.15 | 0.15 | 0.65 | 0.76 | 0.15 | 0.15 |
| Te | 0.27 | 0.51 | 0.40 | 0.30 | 0.17 | 0.17 | 0.50 | 0.30 |
| Sr-Ba | 0.013 | 0.01 | 0.40 | 0.15 | 0.013 | 0.01 | 0.70 | 0.30 |
| Ru | 0.053 | 0.01 | 0.005 | 0.005 | 0.053 | 0.01 | 0.005 | 0.005 |
| La-Ce | 0.01 | 0.0015 | 0.05 | 0.05 | 0.01 | 0.0015 | 0.10 | 0.10 |
| Xe | 1.0 | 1.0 | 0 | 0 | 1.0 | 1.0 | 0 | 0 |

*Adapted from H. P. Nourbakhsh, "Estimate of Radionuclide Release Characteristics Into Containment Under Severe Accident Conditions (Draft for Comment)" NUREG/CR-5747, Brookhaven National Laboratory, December 1991.

**Includes releases due to in-vessel melting, vessel breach, and late revaporization.

# Appendix E. Fractional Release Tables

Table E.1 Grand Gulf — fractional releases and energy deposition rates

| Nuclide group | Whole core inventory* (kg) | Total fraction released into containment** | | Energy deposition rate, $\dot{E}_{dep}$ (MeV/h × $10^{-22}$) | |
|---|---|---|---|---|---|
| | | Low RCS pressure | High RCS pressure | Low RCS pressure | High RCS pressure |
| I | 17.7 | 0.92 | 0.85 | 6.921 | 6.394 |
| Cs | 244.8 | 0.91 | 0.80 | 0.885 | 0.778 |
| Te | 37.1 | 0.67 | 0.67 | 0.499 | 0.499 |
| Sr | 66.7 | 0.71 | 0.713 | 1.480 | 1.486 |
| Ba | 112 | 0.71 | 0.713 | 0.708 | 0.711 |
| Ru | 621 | 0.015 | 0.058 | 0.062 | 0.238 |
| Ce | 1055 | 0.1015 | 0.11 | 0.165 | 0.179 |
| La | 890 | 0.1015 | 0.11 | 2.300 | 2.493 |
| Total | | | | 13.020 | 12.778 |

*From J. A. Gieseke et al., "Radionuclide Release Under Specific LWR Accident Conditions," BMI-2104, Battelle Columbus Laboratories, 1984, and R. S. Denning et al., "Radionuclide Release Calculations for Selected Severe Accident Scenarios," NUREG/CR-4624 (BMI-2139), Battelle Columbus Laboratories, 1986.

**Adapted from H. P. Nourbakhsh, "Estimate of Radionuclide Release Characteristics into Containment Under Severe Accident Conditions (Draft for Comment)," NUREG/CR-5747, Brookhaven National Laboratory, December 1991, assuming limestone concrete.

Table E.2 Peach Bottom — fractional releases and energy deposition rates

| Nuclide group | Whole core inventory* (kg) | Total fraction released into containment** | | Energy deposition rate, $\dot{E}_{dep}$ (MeV/h × $10^{-22}$) | |
|---|---|---|---|---|---|
| | | Low RCS pressure | High RCS pressure | Low RCS pressure | High RCS pressure |
| I | 16.6 | 0.92 | 0.85 | 6.491 | 5.997 |
| Cs | 230.3 | 0.91 | 0.80 | 0.833 | 0.732 |
| Te | 34.9 | 0.67 | 0.67 | 0.469 | 0.469 |
| Sr | 62.7 | 0.71 | 0.713 | 1.391 | 1.397 |
| Ba | 105 | 0.71 | 0.713 | 0.664 | 0.667 |
| Ru | 584 | 0.015 | 0.058 | 0.058 | 0.224 |
| Ce | 992 | 0.1015 | 0.11 | 0.155 | 0.168 |
| La | 836.6 | 0.1015 | 0.11 | 2.162 | 2.343 |
| Total | | | | 12.223 | 11.997 |

*From J. A. Gieseke et al., "Radionuclide Release Under Specific LWR Accident Conditions," BMI-2104, Battelle Columbus Laboratories, 1984, and R. S. Denning et al., "Radionuclide Release Calculations for Selected Severe Accident Scenarios," NUREG/CR-4624 (BMI-2139), Battelle Columbus Laboratories, 1986.

**Adapted from H. P. Nourbakhsh, "Estimate of Radionuclide Release Characteristics into Containment Under Severe Accident Conditions (Draft for Comment)," NUREG/CR-5747, Brookhaven National Laboratory, December 1991, assuming limestone concrete.

Table E.3 Sequoyah — fractional releases and energy deposition rates

| Nuclide group | Whole core inventory* (kg) | Total fraction released into containment** | | Energy deposition rate, $\dot{E}_{dep}$ (MeV/h × $10^{-22}$) | |
|---|---|---|---|---|---|
| | | Low RCS pressure | High RCS pressure | Low RCS pressure | High RCS pressure |
| I | 15.2 | 0.92 | 0.60 | 5.943 | 3.876 |
| Cs | 184.7 | 0.91 | 0.57 | 0.675 | 0.418 |
| Te | 31.7 | 0.92 | 0.67 | 0.579 | 0.426 |
| Sr | 60.9 | 0.41 | 0.413 | 0.780 | 0.786 |
| Ba | 77.7 | 0.41 | 0.413 | 0.284 | 0.286 |
| Ru | 470 | 0.015 | 0.058 | 0.046 | 0.180 |
| Ce | 796 | 0.0515 | 0.06 | 0.063 | 0.074 |
| La | 684 | 0.0515 | 0.06 | 0.897 | 1.045 |
| Total | | | | 9.267 | 7.091 |

*From J. A. Gieseke et al., "Radionuclide Release Under Specific LWR Accident Conditions," BMI-2104, Battelle Columbus Laboratories, 1984, and R. S. Denning et al., "Radionuclide Release Calculations for Selected Severe Accident Scenarios," NUREG/CR-4624 (BMI-2139), Battelle Columbus Laboratories, 1986.

**Adapted from H. P. Nourbakhsh, "Estimate of Radionuclide Release Characteristics into Containment Under Severe Accident Conditions (Draft for Comment)," NUREG/CR-5747, Brookhaven National Laboratory, December 1991, assuming limestone concrete.

Table E.4 Surry TMLB′ — fractional releases and energy deposition rates

| Nuclide group | Whole core inventory* (kg) | Total fraction released into containment** | | Energy deposition rate, $\dot{E}_{dep}$ (MeV/h × $10^{-22}$) | |
|---|---|---|---|---|---|
| | | Low RCS pressure | High RCS pressure | Low RCS pressure | High RCS pressure |
| I | 12.4 | 0.92 | 0.60 | 4.848 | 3.162 |
| Cs | 145.7 | 0.92 | 0.57 | 0.532 | 0.330 |
| Te | 25.4 | 0.81 | 0.57 | 0.413 | 0.290 |
| Sr | 47.6 | 0.16 | 0.163 | 0.238 | 0.242 |
| Ba | 61.2 | 0.16 | 0.163 | 0.087 | 0.089 |
| Ru | 369 | 0.015 | 0.058 | 0.037 | 0.142 |
| Ce | 626 | 0.0515 | 0.06 | 0.050 | 0.058 |
| La | 539 | 0.0515 | 0.06 | 0.707 | 0.823 |
| Total | | | | 6.912 | 5.136 |

*From J. A. Gieseke et al., "Radionuclide Release Under Specific LWR Accident Conditions," BMI-2104, Battelle Columbus Laboratories, 1984, and R. S. Denning et al., "Radionuclide Release Calculations for Selected Severe Accident Scenarios," NUREG/CR-4624 (BMI-2139), Battelle Columbus Laboratories, 1986.

**Adapted from H. P. Nourbakhsh, "Estimate of Radionuclide Release Characteristics into Containment Under Severe Accident Conditions (Draft for Comment)," NUREG/CR-5747, Brookhaven National Laboratory, December 1991, assuming basaltic concrete.

NUREG/CR-5732
ORNL/TM-11861
Dist. Category R3

## INTERNAL DISTRIBUTION

1. W. S. Aaron
2. C. W. Alexander
3. F. Barrera
4-8. E. C. Beahm
9. J. T. Bell
10. D. O. Campbell
11. J. L. Collins
12. W. Fulkerson
13. R. K. Genung
14. J. R. Hightower
15. E. K. Johnson
16. M. J. Kania
17-21. T. S. Kress
22. R. A. Lorenz
23. J. C. Mailen
24. M. F. Osborne
25-29. G. W. Parker
30. C. E. Pugh
31. M. G. Stewart
32. R. P. Taleyarkhan
33-37. C. F. Weber
38. Central Research Library
39. ORNL—Y-12 Technical Library Document Reference Section
40-41. Laboratory Records
42. Laboratory Records, ORNL RC
43. ORNL Patent Section

## EXTERNAL DISTRIBUTION

44. Office of Assistant Manager for Energy Research and Development, DOE-OR, P.O. Box 2001, Oak Ridge, TN 37831
45. Director, Division of Reactor Safety Research, U.S. Nuclear Regulatory Commission, Washington, DC 20555
46-47. Office of Scientific and Technical Information, P.O. Box 2001, Oak Ridge, TN 37831
48. Division of Technical Information and Document Control, U.S. Nuclear Regulatory Commission, Washington, DC 20555
49. R. Y. Lee, Accident Evaluation Branch, U.S. Nuclear Regulatory Commission, NLN-353, Washington, DC 20555
50. R. O. Meyer, U.S. Nuclear Regulatory Commission, Nuclear Regulatory Research, NLS-007, Washington, DC 20555
51. F. Eltawila, Accident Evaluation Branch, U.S. Nuclear Regulatory Commission, NLN344, Washington, DC 20555
52. K. S. Norwood, 8 Appleford Drive, Abingdon, Oxon OX14, 2DA, United Kingdom
53. S. J. Wisbey, B.220, AERE Harwell, Didcot, Oxon OX11 ORA, United Kingdom
54. T. Yamashita, Nuclear Fuel Chemistry Laboratory, Department of Chemistry, Japan Atomic Energy Research Institute, Tokai-mura, Naka-gun, Ibaraki-ken, 319-11, Japan
55. S. Hagen, Bau 601, Kernforschungszentrum Karlsruhe, Postface 3640, D7500 Karlsruhe 1, Federal Republic of Germany
56. M. L. Brown, 15 Barrock St., Thurso Caithness, Scotland KW14 7DB
57. T. Nakamura, Reactivity Accident Laboratory, Dai-2-Genken-Shinhara-Jutaku-304, 1-23-5, Shinhara, Mito-shi, 310, Japan
58. H. K. Lee, Spent Fuel Storage and Disposal Technology Section, Korea Advanced Energy Research Institute, P.O. Office Box 7, Dae-Danji Choong-Nam, Republic of Korea
59. Y.-C. Tong, Institute of Nuclear Energy Research, P.O. Box 3-6, Lung-Tan, Taiwan, Republic of China
60. D. Williams, Technology Division, AEE Winfrith, Dorchester, Dorset, England
61. F. C. Inglesias, AECL, Chalk River Nuclear Laboratories, Chalk River, Ontario, KOJ 1JO, Canada
62. R. R. Hobbins, EG&G Idaho, Inc., P.O. Box 1625, Idaho Falls, ID 83401
63. D. A. Petti, EG&G Idaho, Inc., P.O. Box 1625, Idaho Falls, ID 83401

64. D. J. Osetek, Sandia National Laboratory, P.O. Box 5800, Albuquerque, NM 87185
65. K. O. Reil, Sandia National Laboratory, P.O. Box 5800, Albuquerque, NM 87185
66. D. Powers, Sandia National Laboratory, P.O. Box 5800, Albuquerque, NM 87185
67. L. A. Neimark, Argonne National Laboratory, 9700 South Cass Ave., Argonne, IL 60439
68. J. Rest, Argonne National Laboratory, 9700 South Cass Ave., Argonne, IL 60439
69. Y. Y. Liu, Argonne National Laboratory, 9700 South Cass Ave., Argonne, IL 60439
70. C. A. Alexander, Battelle Memorial Institute, 505 King Ave., Columbus, OH 43201
71. F. Panisko, Pacific Northwest Laboratory, P.O. Box 999, Richland, WA 99352
72. K. Y. Suh, Fauske & Associates, Inc., 16W070 West 83rd St., Burr Ridge, IL 60521

73-322. Given distribution as shown in Category R3 (NTIS - 10)

NRC FORM 335 (2-89) NRCM 1102, 3201, 3202

U.S. NUCLEAR REGULATORY COMMISSION

# BIBLIOGRAPHIC DATA SHEET

*(See instructions on the reverse)*

1. REPORT NUMBER (Assigned by NRC, Add Vol., Supp., Rev., and Addendum Numbers, if any.)

NUREG/CR-5732
ORNL/TM-11861

2. TITLE AND SUBTITLE

Iodine Chemical Forms in LWR Severe Accidents

Final Report

3. DATE REPORT PUBLISHED

| MONTH | YEAR |
|---|---|
| April | 1992 |

4. FIN OR GRANT NUMBER

B0854

5. AUTHOR(S)

E. C. Beahm, C. F. Weber, T. S. Kress, and G. W. Parker

6. TYPE OF REPORT

Technical

7. PERIOD COVERED *(Inclusive Dates)*

8. PERFORMING ORGANIZATION – NAME AND ADDRESS *(If NRC, provide Division, Office or Region, U.S. Nuclear Regulatory Commission, and mailing address; if contractor, provide name and mailing address.)*

Oak Ridge National Laboratory
Oak Ridge, TN 37831-6285

9. SPONSORING ORGANIZATION – NAME AND ADDRESS *(If NRC, type "Same as above"; if contractor, provide NRC Division, Office or Region, U.S. Nuclear Regulatory Commission, and mailing address.)*

Division of Systems Research
Office of Nuclear Regulatory Research
U.S. Nuclear Regulatory Commission
Washington, DC 20555

10. SUPPLEMENTARY NOTES

11. ABSTRACT *(200 words or less)*

Calculated data from seven severe accident sequences in light water reactor plants were used to assess the chemical forms of iodine in containment. In most of the calculations for the seven sequences, iodine entering containment from the reactor coolant system was almost entirely in the form of CsI with very small contributions of I or HI. The largest fraction of iodine in forms other than CsI was a total of 3.2% as I plus HI. Within the containment, the CsI will deposit onto walls and other surfaces, as well as in water pools, largely in the form of iodide ($I^-$). The radiation-induced conversion of $I^-$ in water pools into $I_2$ is strongly dependent on pH. In systems where the pH was controlled above 7, little additional elemental iodine would be produced in the containment atmosphere. When the pH falls below 7, however, it may be assumed that it is not being controlled and large fractions of iodine as $I_2$ within the containment atmosphere may be produced.

12. KEY WORDS/DESCRIPTORS *(List words or phrases that will assist researchers in locating the report.)*

iodine
fission product behavior
reactor containment
severe accidents
LWRs

13. AVAILABILITY STATEMENT

unlimited

14. SECURITY CLASSIFICATION

*(This Page)*

unclassified

*(This Report)*

unclassified

15. NUMBER OF PAGES

16. PRICE